JOC The Journal of Organic Chemistry
Cite This: J. Org. Chem. 2019, 84, 9101−9116
Article
pubs.acs.org/joc

Photoactive Boron−Nitrogen−Carbon Hybrids: From Azo-borazines to Polymeric Materials

Hamid Oubaha,[†,‡] Nicola Demitri,[§] Joëlle Rault-Berthelot,[∥] Philippe Dubois,[‡] Olivier Coulembier,[*,‡] and Davide Bonifazi[*,†,⊥]

[†]Department of Chemistry, University of Namur, Rue de Bruxelles 61, 5000 Namur, Belgium
[‡]Laboratory of Polymeric and Composite Materials (LPCM), Center of Innovation and Research in Materials and Polymers (CIRMAP), University of Mons, Place du Parc 23, 7000 Mons, Belgium
[§]Elettra-Sincrotrone Trieste, S.S. 14 Km 163.5 in Area Science Park, 34149 Basovizza, Trieste, Italy
[∥]Univ. Rennes, CNRS, ISCR-6226, F-35000 Rennes, France
[⊥]School of Chemistry, Cardiff University, Main Building, Park Place, Cardiff CF10 3AT, United Kingdom

Supporting Information

ABSTRACT: In this paper, we describe synthetic routes for preparing a novel switchable BNC-based chromophore, composed of a borazine core peripherally functionalized with azobenzene moieties. Capitalizing on the Pd-catalyzed Suzuki cross-coupling reaction between a tris-triflate borazine and an organoboron azobenzene derivative, a photoswtichable azo-borazine derivative was successfully prepared. The molecule showed reversible E/Z photoisomerization upon irradiation at the maximum of the intense $\pi-\pi^*$ absorption feature (360 nm). X-ray crystallographic investigations revealed a nonplanar orientation of the three azobenzene moieties and the trans configuration of the −N═N− bonds. Building on the synthetic versatility of the borazine-azobenzene derivative, we used this photoactive scaffold to engineer soluble BN-doped polythiophene polymers. Photophysical characterization performed in solvents of different polarity suggested that the polymer undergoes intramolecular charge transfer (ICT).

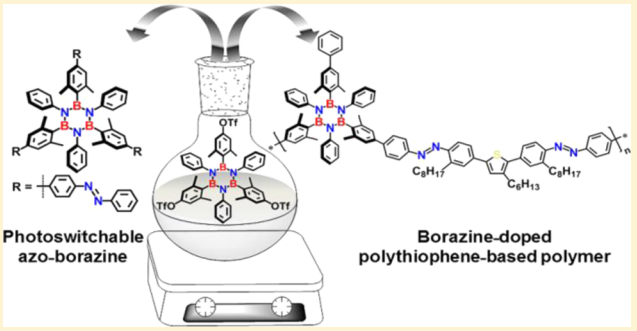

INTRODUCTION

Stimuli-responsive molecules and materials capable of undergoing reversible structural changes are of great interest for future technology.[1] A typical example is the E/Z photoisomerization of azobenzenes, which is characterized by an irradiation-induced $Z \rightarrow E$ isomerization between the thermodynamically favored, stretched E-isomer and its Z-isomer. The photoisomerization is accompanied by a dramatic change in electronic structure, geometric shape, and polarity, resulting into the spatiotemporal control of the conformational and overall structural properties of molecular systems.[2] Notable applications include their integration into architectures expressing functional properties in materials science,[3] biology,[4] and molecular recognition.[1c,5]

The replacement of C═C units by more polarized BN couples is a versatile functionalization strategy to tailor the optoelectronic characteristics of organic π systems without significant structural alteration of the nanostructure.[6] The BN/CC isosterism concept goes back to the seminal discovery of borazine ($H_3B_3N_3H_3$) by Stock and Pohland in 1926.[7] The borazine core is commonly referred to as the "inorganic benzene", owing to its iso-electronic and iso-structural relationships with benzene.[7] Accordingly, borazine and its derivatives are valuable scaffolds to be inserted as doping units in graphitic-based carbon materials to tailor their optoelectronic characteristics[8] and self-assembly properties on surfaces.[9,23] Important examples include dendritic borazine-doped polyphenylenes,[10] borazine-doped coronenes,[11] and borazino-based polymers.[10,12] Not only borazine-based materials but also hybrid BNC-based architectures are attracting increasing consideration due to their thermal stability, mechanical robustness, and tunable optoelectronic properties.[13] In this respect, the incorporation of BN units into π-conjugated polymers is emerging as an evident route to broaden the scope of organic electronic materials.[6d,13b,14] For their part, π-conjugated polymers have revolutionized the field of optoelectronics[15] and are nowadays used to produce low-cost, large-area, and flexible electronic devices.[16] In these materials, the tailoring of the lowest unoccupied molecular orbital (LUMO)/highest occupied molecular orbital (HOMO) energy levels for a given application is of high importance.[15d,17] Among the different strategies, the incorporation of heteroatomic units into polymer structures such as boron and nitrogen atoms revealed to be a powerful strategy to prepare isostructural

Received: April 16, 2019
Published: June 20, 2019

DOI: 10.1021/acs.joc.9b01046
J. Org. Chem. 2019, 84, 9101−9116

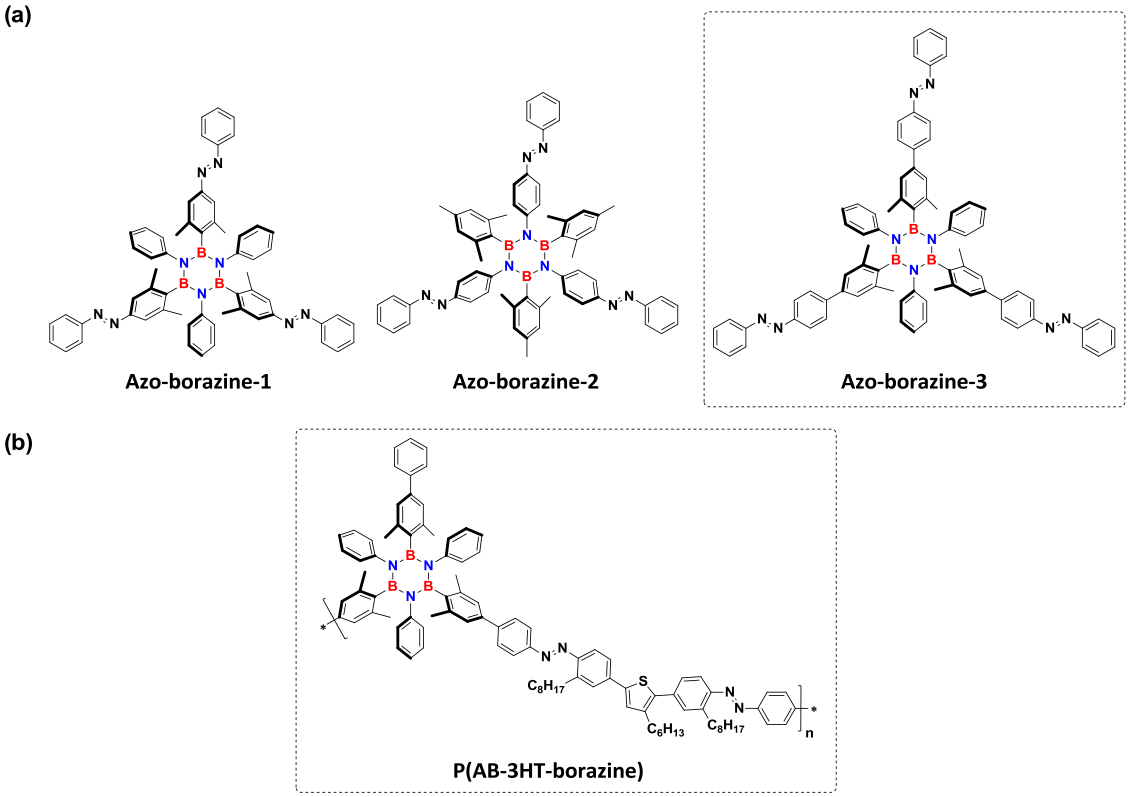

Figure 1. Molecular structures of the targeted borazine-based BNC molecules and hybrid polymers.

Scheme 1. Synthetic Approach toward the Preparation of Azobenzene-borazine-Based BNC Hybrid Materials[a]

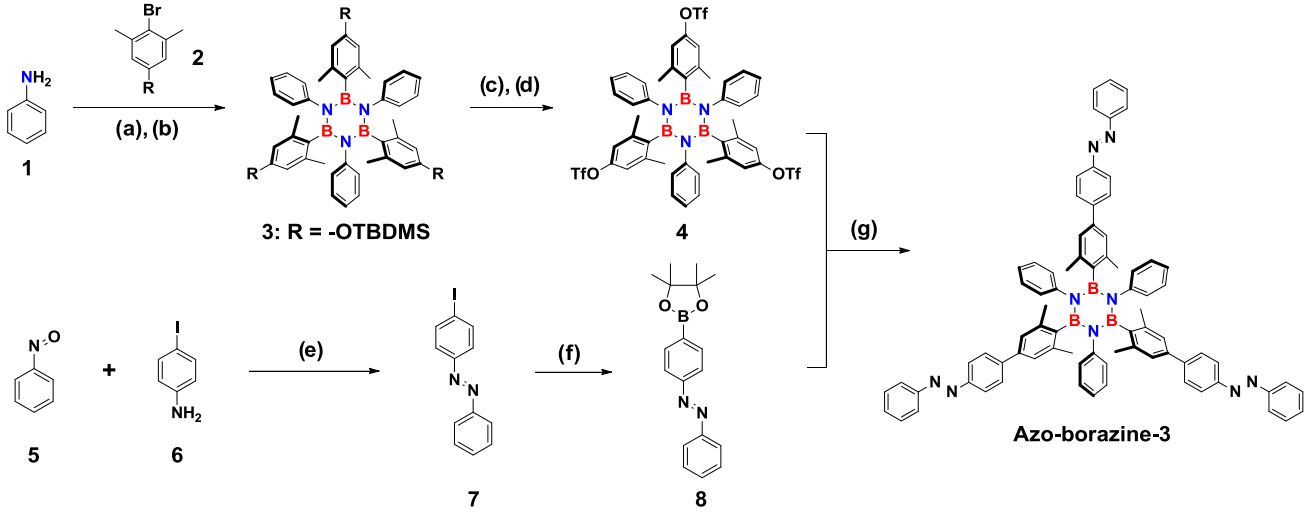

[a]Reagents and conditions: (a) BCl_3, toluene, reflux, 18 h; (b) **2**, *tert*-BuLi, THF, −84 °C to rt, 16 h, 49%; (c) TBAF, THF, 0 °C, 2 h; (d) Tf_2O, pyridine, rt, 16 h, 75%; (e) AcOH, rt, 18 h, 81%; (f) B_2Pin_2, KOAc, [Pd(dppf)Cl_2·CH_2Cl_2], DMF, 80%; (g) K_2CO_3, [Pd(PPh_3)$_4$], 1,4-dioxane/H_2O (3:1 v/v), 105 °C, 18 h, 83%. TBAF: tetra-butylammonium fluoride. Tf_2O: tri-fluoromethanesulfonic anhydride. B_2Pin_2: 4,4,4′,4′,5,5,5′,5′-Octamethyl-2,2′-bi-1,3,2-dioxaborolane. [Pd(dppf)Cl_2·CH_2Cl_2]: [1,1′-bis(diphenylphosphino)ferrocene dichloropalladium(II)] dichloromethane adduct.

molecular[6c,11,18] and polymeric materials[6d,14a,19] bearing strong local dipole moments.[14a,b,20]

Owing to the possibility of functionalizing the borazine core with different groups on the aryl substituents at the N and B atoms[6e,7d,21] and to the easy polymerization of thiophenes for producing low-cost and flexible electronic devices, we have envisaged to employ borazine (B_3N_3) as the core skeleton and azobenzene as the photoresponsive unit to engineer new photoswitchable molecular BNC hybrid materials (Figure 1). Considering the conductive properties of poly(3-hexylthiophene) (P3HT),[22] the 3-hexylthiophene scaffold was selected as a monomeric unit to develop the polymer material. Also, we were not unmindful to exploiting the side alkyl chains to enhance the solubility of the final material (Figure 1b).

DOI: 10.1021/acs.joc.9b01046
J. Org. Chem. 2019, 84, 9101−9116

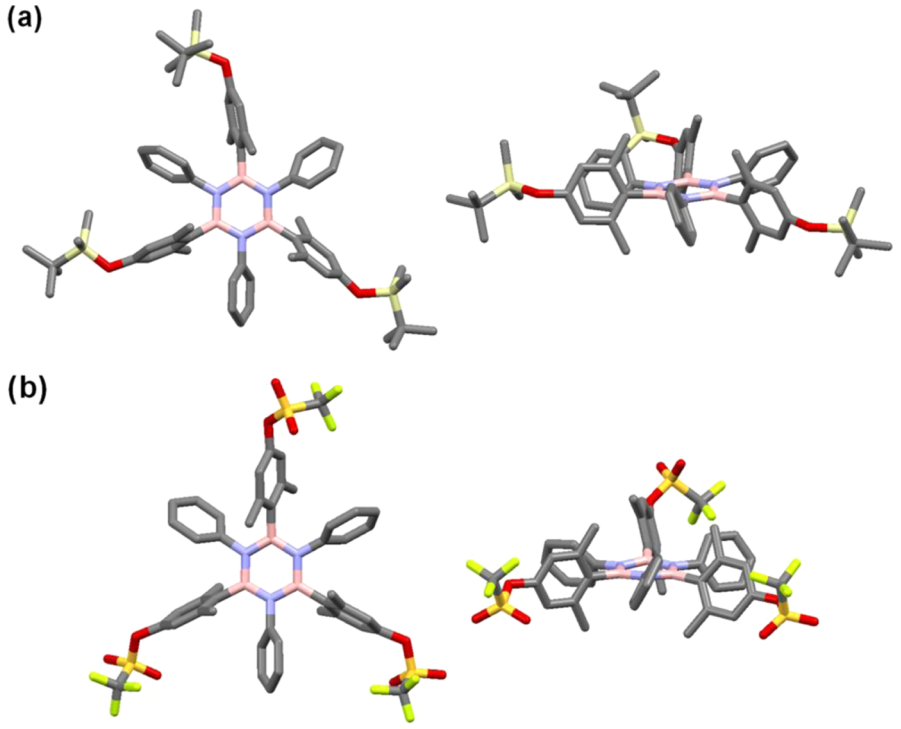

Figure 2. X-ray-determined molecular structure of (a) compound **3** and (b) compound **4** (atom colors: blue N, pink B, red O, yellow Si, orange S, light green F, and gray C; hydrogen atoms are omitted for clarity). Space group: (a) $P\bar{1}$ (b) $P2_1/n$.

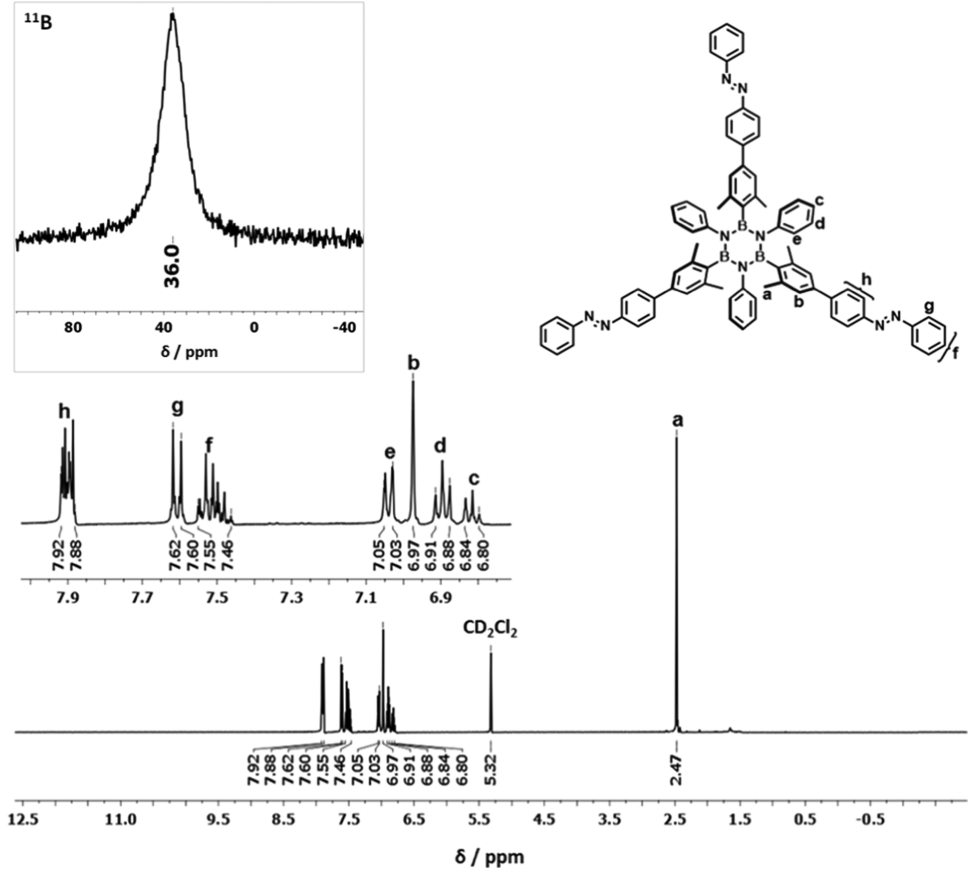

Figure 3. ^{1}H NMR spectrum of **azo-borazine-3** (CD_2Cl_2, 400 MHz, 25 °C). Inset: a zoom of the region 6.60−8.00 ppm and ^{11}B NMR spectrum ($CDCl_3$, 128 MHz, 25 °C).

DOI: 10.1021/acs.joc.9b01046
J. Org. Chem. 2019, 84, 9101−9116

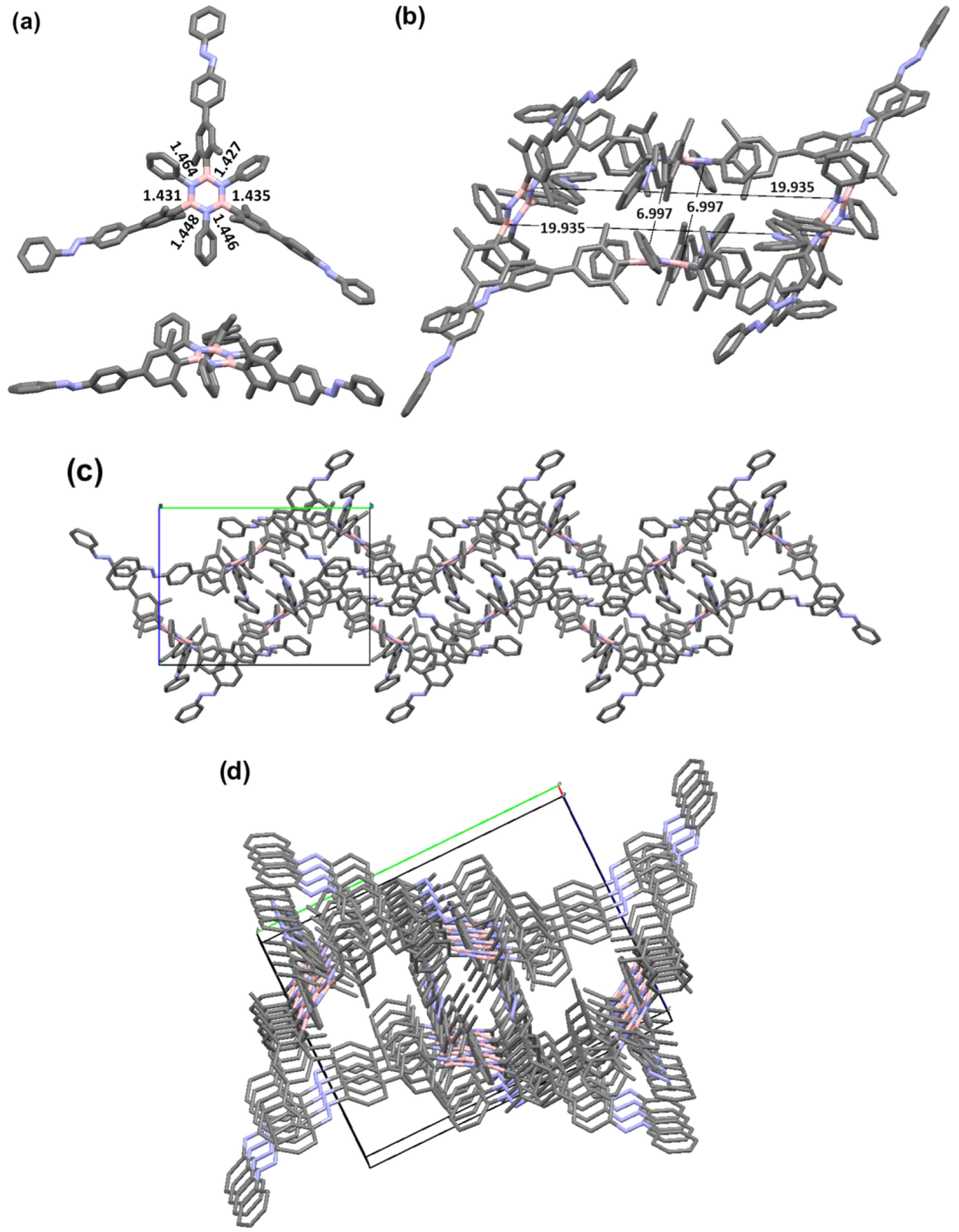

Figure 4. (a) Frontal (top) and side (bottom) views of the X-ray crystal structure of **azo-borazine-3** (with the B−N distances in Å), (b) packing diagram viewed along the *a* axis, (c) crystal packing, along the *a* crystallographic direction, showing a zigzag stacking shape of the molecules, and (d) adjacent layers stack forming a three-dimensional porous assembly. (Atom colors: blue N, pink B, gray C; hydrogen atoms are omitted for clarity). Space group: $P2_1/c$.

RESULTS AND DISCUSSION

Synthesis the Azo-borazine Core. Three classes of derivatives were targeted as photoactive BNC molecular scaffold: **azo-borazine-1**, **azo-borazine-2**, and **azo-borazine-3** (Figure 1a). Due to the chemical sensitivity of the B_3N_3 core under the reaction conditions to form azobenzene moiety, **azo-borazine-1** and **azo-borazine-2** could not be prepared (see the Supporting Information for the attempts). Thus, we decided to follow a convergent synthetic pathway, in which a precursor B_3N_3 core is reacted with azobenzene moieties, avoiding the need to use strong oxidizing conditions to form the azo-functional group. It is following this approach that we prepared **azo-borazine-3** reacting a suitable aryl halide or related electrophile (i.e., ArOTf) with an organoboron derivative of a given azobenzene under Suzuki cross-coupling reaction conditions (Scheme 1). Specifically, *tert*-butyldimethylsilyl (TBDMS)-protected borazine derivative **3** was prepared following a modified protocol[8,23] of that reported by Groszos and Stafiej[24] and later by Yamaguchi.[21] The synthesis started with the reaction of aniline **1** with BCl_3 under refluxing conditions giving the intermediate tri-*B*-chloro-tri-*N*-phenyl-borazine that, upon reaction with TBDMS-protected ArLi, could be transformed into TBDMS-protected borazine derivative **3** in 49% yield (reactions a and b). Removal of the TBDMS protecting group with TBAF and successive esterification with Tf_2O in pyridine led to the key intermediate tris-triflate borazine **4** in 75% yield (reactions c and d).[10] White suitable crystals were obtained from evaporation of a solution containing either compound **3** (Figure 2a) or compound **4**

DOI: 10.1021/acs.joc.9b01046
J. Org. Chem. 2019, 84, 9101−9116

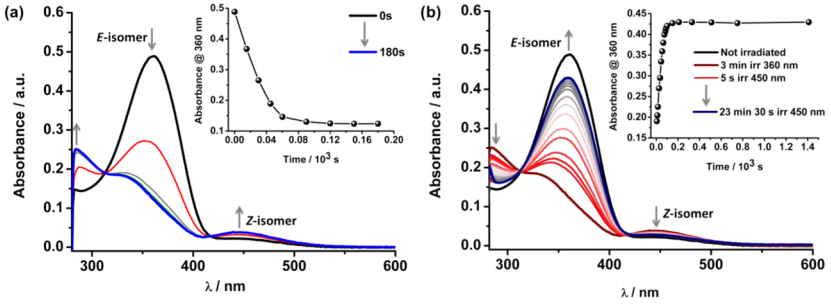

Figure 5. Reversible change in the absorption spectra of a 5×10^{-6} M solution of **azo-borazine-3** in toluene under irradiation at (a) 360 nm and (b) 450 nm at rt (23 °C). Inset: UV absorption at 360 nm of **azo-borazine-3** in toluene as a function of irradiation time.

(Figure 2b) in $CHCl_3$ belonging to the $P\bar{1}$ and $P2_1/n$ space groups, respectively. As expected, the X-ray molecular structures show the quasi-orthogonal arrangement of the aryl moieties, which place the methyl substituents atop the B atoms, sterically shielding the electrophilic B centers.[25] In parallel, the synthesis of the organoboron derivative of azobenzene **8** was performed through the Mills reaction, starting from commercially available nitrosobenzene **5** and 4-iodoaniline **6** followed by a Miyaura borylation reaction (Scheme 1, reactions e and f). The final Suzuki cross-coupling reaction between borazine **4** and azobenzene-boronic ester **8** yielded desired **azo-borazine-3** in 83% yield (Scheme 1, reaction g).

Azo-borazine-3 derivative was characterized using NMR, IR, and MALDI-ToF spectrometry. At first, **azo-borazine-3** was identified by MALDI-ToF through the detection of the peak corresponding to the molecular ion at m/z 1162.6010 ($[M + H]^+$) (calcd for $C_{78}H_{67}B_3N_9^+$ 1162.5793). ^{1}H NMR analysis further confirmed the chemical structure (Figure 3) and the ^{11}B NMR spectrum showed a broad peak at 36.0 ppm (inset Figure 3), consistent with a boron atom substituted by two N atoms and linked to one carbon atom. Finally, the IR spectrum revealed an intense band at 1353 cm^{-1}, characteristic of the B−N stretching in a borazine core.[8]

Small needlelike orange crystals of **azo-borazine-3** suitable for X-ray diffraction were grown by vapor diffusion of hexane to a solution of **azo-borazine-3** in CH_2Cl_2. Similar to borazine **4**, the X-ray molecular structure shows the quasiorthogonal arrangement of the aryl moieties. The X-ray analysis confirms the trans configuration of the −N═N− functional groups and reveals the nonplanar arrangement of the three aryl rings in the solid state (Figure 4a). A deviation from an orthogonal arrangement of the aryl substituents and the borazine ring is clearly observed with interplanar angles of 122.6° between the borazine ring and phenyl groups and of 108.9° between both phenyl and xylyl groups. As previously observed in the literature,[8,25] the intra-annular distance values between boron and nitrogen atoms are between 1.43 and 1.46 Å, with the internal angle of the borazine cycle between 122.7 and 117.03° (BNB and NBN, respectively).

Notably, the azobenzene moieties in the crystal exist in a twisted shape with respect to the B-aryl groups (Figure 4a). Interestingly, the crystal packing four **azo-borazine-3** molecules stack in a parallelepiped-like fashion. The borazine cores constitute the four faces of the arrangement, with each B-center facing the N-center forming layers separated by a distance of 6.99 and 19.93 Å (Figure 4b). Each layer is formed by borazine molecules lying side by side on the same plane and separated by a distance of 20.22 Å (Figure 4c), and the adjacent layers are assembled in a zigzag-like stacking forming a three-dimensional porous assembly (Figure 4d).

Photo- and Thermal Isomerizations of Azo-borazine-3. The photoisomerization reaction between the *E*- and *Z*-isomers of **azo-borazine-3** was studied in toluene (5×10^{-6} M) at room temperature (rt) (Figure 5). The molecule exhibits two UV absorption bands at 360 and 450 nm, which are attributed to $\pi-\pi^*$ (of the *E*-isomer) and $n-\pi^*$ (of the *Z*-isomer) electronic transitions, respectively.[2b,26] When irradiated at 360 nm, remarkable changes are observed in the absorption spectra of **azo-borazine-3** (Figure 5a), with an intense and fast increase of a new band centered at around 290 nm and a substantial increase of the intensity of the $n-\pi^*$ band at 450 nm (inset of Figure 5a) with a concomitant disappearance of the $\pi-\pi^*$ absorption band. Neat isosbestic points are maintained throughout the photoirradiation experiments, showing the clean occurrence of the nearly quantitative $E \rightarrow Z$ isomerization after 3 min of irradiation, whereas no evolution in the UV−vis absorption was observed even after 20 min of irradiation at 360 nm. On the other hand, irradiation at 450 nm causes the $Z \rightarrow E$ isomerization, as observed by the simultaneous decrease and increase of the $n-\pi^*$ and $\pi-\pi^*$ absorption bands, respectively. Full restoration of the *E*-isomer was not observed even after 23 min of irradiation at 450 nm (Figure 5b).

Repetitive photoinduced switching cycles evidenced excellent fatigue resistance and remarkable photostability of **azo-borazine-3** (Figure 6). As expected, the borazine core has little

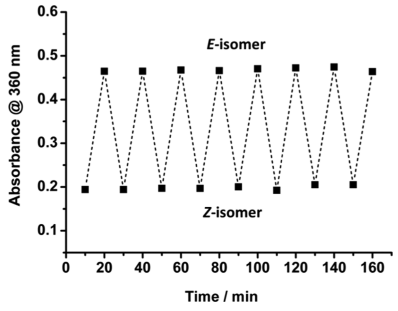

Figure 6. Repetitive photoinduced switching cycles of the **azo-borazine-3** obtained by alternating irradiations at 360 and 450 nm (5×10^{-6} M solution in toluene at 23 °C).

influence on the photochemical properties, with **azo-borazine-3** showing the typical *E*/*Z* switching behavior of standard azobenzenes.[2b,27] The UV-absorbing BN-core does not interfere with the excitation properties of the azobenzene moieties. The thermal $Z \rightarrow E$ isomerization (obtained after irradiation at 360 nm for 3 min) was realized by measuring the absorbance of a 5×10^{-6} M solution of **azo-borazine-3** in toluene at different temperatures (Figure 7a). As shown in Figure 7, the thermal *Z*

DOI: 10.1021/acs.joc.9b01046
J. Org. Chem. 2019, 84, 9101−9116

→ *E* interconversion occurs very slowly and the spectral profile of the *E*-isomer is fully recovered only upon heating at 100 °C.

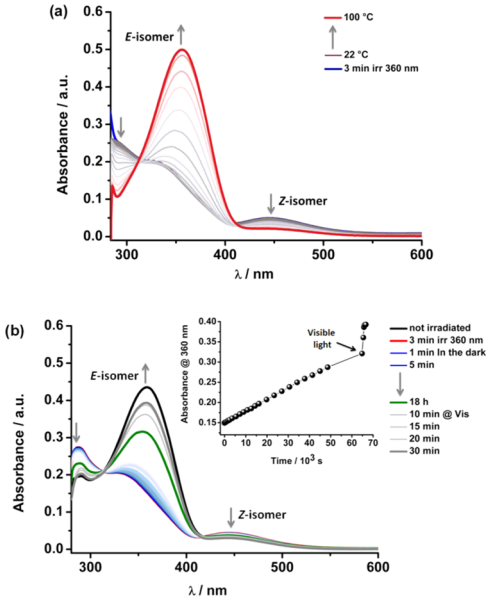

Figure 7. UV−vis measurements of the thermal $Z \rightarrow E$ isomerization of **azo-borazine-3** after sample irradiation at 360 nm (5×10^{-6} M in toluene) (a) and at rt in the dark (b).

Self-Assembly Behavior of Azo-borazine-3. To investigate the aggregation properties of **azo-borazine-3**, a THF/water mixture solvent was used to trigger the self-assembly into nanoparticles. Particles were formed by dissolving **azo-borazine-3** in THF containing various fractions (f_w) of water at a concentration of 4.6×10^{-6} M under sonication at 40 °C for 15 min. As shown in Figure 8a, in pure THF, the absorption spectra of the **azo-borazine-3** consist of a strong absorption peak at 360 nm and a very weak band around 450 nm attributed to $\pi-\pi^*$ and $n-\pi^*$ electronic transitions of the azobenzene unit, respectively. Upon increasing the water fraction, the absorption spectra broadened and showed a hypochromic effect in intensity, suggesting the formation of aggregates.[28] Similarly, emission measurements were recorded for **azo-borazine-3** under excitation at 360 nm (Figure 8b). **Azo-borazine-3** in THF exhibits an emission maximum at 406 nm with a fluorescence quantum yield (Φ_{fl}) of 0.82%. An appreciable enhancement of the emission intensity was observed with increasing fractions of water, with the maximum being at 406 nm (Φ_{fl} = 3.28%, f_w = 95%). In these compounds, intramolecular rotations play a crucial role in populating the nonradiative decay channels for the excited states and enhance their rates.[29] The free intramolecular torsional motion in solution favors nonradiative decays that are responsible for the weak emission in THF.[30] However, these torsional motions are hindered in the aggregated state. The enhancement of the emission in the aggregated state also suggested suppression of the concentration quenching in the aggregated state by amplified intermolecular distances resulting from the partially distorted structure of the fluorogenic units.[31]

Then, we investigated the morphology of the as-formed aggregates using a transmission electron microscope (TEM). Spherical aggregates with different diameters from 90 to ∼600 nm were obtained for samples containing **azo-borazine-3** prepared in a THF/H_2O mixture (f_w = 95%) (Figure 9a−d). Notably, some of the particles stick together to form large aggregates (Figure 9e). Dynamic light scattering measurements (Figure 9f) performed on the same sample confirmed the presence of aggregates displaying hydrodynamic diameters ranging from 110 ± 20 to 295 ± 150 nm, together with larger particles with hydrodynamic diameters of 4 ± 1 μm. Since the formation of the nanoparticles involves stepwise addition of a poor solvophobic solvent (H_2O) to a stable solution of the **azo-borazine-3** in THF, the solubility of the molecule is gradually reduced upon addition of water, leading to the formation of aggregates. Larger nanoparticles are formed either through attractive vdW or dipolar forces. As previously suggested by Ajayaghosh and co-workers for azobenzene-based nanodots,[3g] the growth of these aggregates could also be attributed to a light-driven "Ostwald ripening"-type mechanism.[32]

Synthesis of the Borazine-Doped Polythiophene-Based Polymer. For the application of azo-borazine as a building block in the polymer main chain, the key issue is to introduce reactive groups on repetitive units. Therefore, we synthesized bis-triflate borazine derivative (bis-OTf-borazine) **9** starting from the tris-OTf-borazine **4** and azobenzene-functionalized thiophene derivative ((1*E*,1′*E*)-2,2′-((3-hexylthiophene-2,5-diyl)bis(2-octyl-4,1-phenylene))bis(1-(4-(4,4,5,5-tetramethyl-1,3,2-dioxaborolan-2-yl)phenyl)diazene)) (AB-3HT-$(BPin)_2$) **21** as monomers. Bis-OTf-borazine **9** was prepared in 30% yield via a Suzuki cross-coupling reaction between tris-OTf-borazine **4** and phenylboronic acid (Scheme 2, reaction a). In parallel, AB-3HT-$(BPin)_2$ **21** monomer was prepared starting from 1-bromo-2-nitrobenzene **10** and 1-octyne through a Sonogashira cross-coupling reaction leading to 1-nitro-2-(oct-1-yn-1-yl)-benzene **11** in 90% yield (Scheme 2, reaction b). Compound **11** was quantitatively reduced using Pd-catalyzed hydrogenation yielding compound **12** (Scheme 2, reaction c).

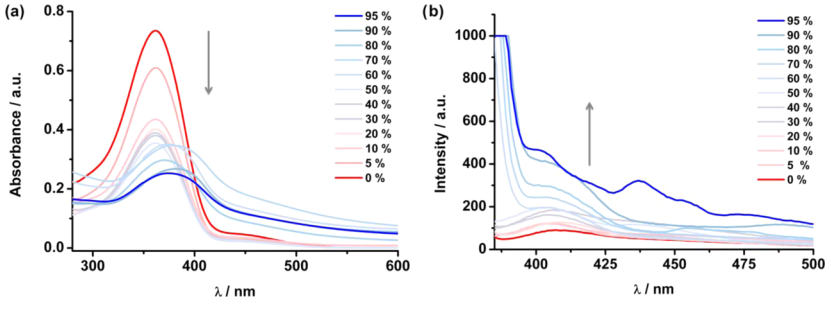

Figure 8. (a) Absorption and (b) fluorescence ($\lambda_{excitation}$ = 360 nm) spectra of the **azo-borazine-3** in THF with increasing water contents (f_w %) recorded at rt (the final concentration was 4.6×10^{-6} M).

DOI: 10.1021/acs.joc.9b01046
J. Org. Chem. 2019, 84, 9101−9116

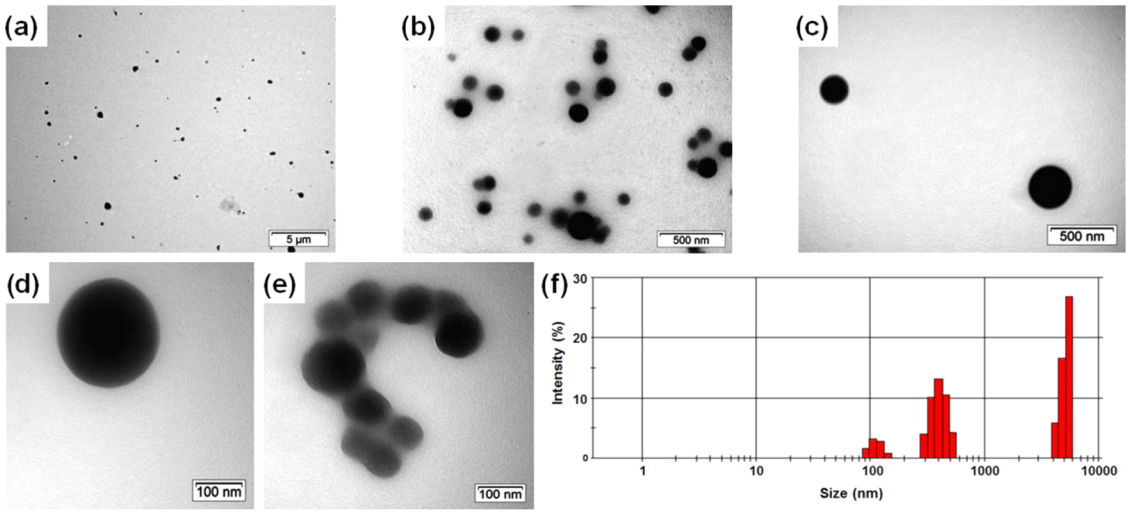

Figure 9. (a–e) TEM images of **azo-borazine-3** prepared from THF solution with 95% water and (f) average size of the particles as measured by dynamic light scattering (4.6×10^{-6} M, f_w = 95%).

Regioselective bromination of **12** by pyridinium hydrobromide perbromide gave 4-bromo-2-octylaniline **13** in 71% yield (Scheme 2, reaction d). Miyaura borylation of compound **13** in 1,4-dioxane provided 2-octyl-4-(4,4,5,5-tetramethyl-1,3,2-dioxaborolan-2-yl)aniline **14** in 50% yield (Scheme 2, reaction e). Compound **14** was then coupled to 3-hexyl-2,5-diiodothiophene **16**, prepared in 90% yield from 3-hexylthiophene **15** (Scheme 2, reaction f), via the Suzuki cross-coupling reaction yielding (4,4′-(3-hexylthiophene-2,5-diyl)bis(2-octylaniline)) **17** in 30% yield (Scheme 2, reaction g). Compound **17** was reacted with 1-bromo-4-nitrosobenzene **19**, prepared from 4-bromoaniline **18** (Scheme 2, reaction h), using Mills reaction conditions[33] giving access to (1*E*,1′*E*)-2,2′-((3-hexylthiophene-2,5-diyl)bis(2-octyl-4,1-phenylene))bis(1-(4-bromophenyl)-diazene) AB-3HT-Br_2 **20** in 45% yield (Scheme 2, reaction i). Miyaura borylation of compound **20** led to the desired monomer AB-3HT-$(BPin)_2$ **21** in 65% yield (Scheme 2, reaction j). Finally, the synthesis of the **P(AB-3HT-borazine)** polymer was carried out using a standard Suzuki cross-coupling polycondensation reaction (Scheme 2, reaction k). The molecular weight estimated by gel permeation chromatography (GPC) relative to polystyrene standard in THF (+2% Et_3N) at 30 °C was 13.2 kDa with a dispersity ($Đ_M$) of 1.92 and a degree of polymerization (DP) of 9.

The polymer is soluble in common organic solvents, such as CH_2Cl_2, chloroform, THF, and toluene, and insoluble in acetone, methanol, and *n*-heptane. ^{1}H NMR spectrum of **P(AB-3HT-borazine)** polymer in $CDCl_3$ (Figure 10) showed all characteristic peaks of its repeating units. The low-field shifting of the aromatic proton resonance of the (OTf)-aryl group of the borazine unit from 6.49 ppm in the starting material (bis-OTf-borazine) to 6.92 ppm in the polymer structure suggests that the desired polymer has been formed. As revealed by thermogravimetric analysis (Supporting Information, Figure S25), **P(AB-3HT-borazine)** polymer exhibits good thermal stability with a mass loss of 5 wt % starting at 203 °C and a loss of about 30 wt % at 351 °C. On the other hand, differential scanning calorimetry analysis performed from −25 to 200 °C showed glass transition (T_g) at about 112 °C. Moreover, no melting and crystallization peaks were detected, suggesting the amorphous nature of the polymer (Supporting Information, Figure S26).

The absorption spectra of monomers bis-OTf-borazine **9**, AB-3HT-$(BPin)_2$ **21** as well as **P(AB-3HT-borazine)** polymer in solutions and in thin films are depicted in Figure 11.

Absorption spectra of borazine unit either in solution or in film gave predominately one band at 268 and 266 nm, respectively, corresponding to S_0-S_1 transition. Absorption spectra of thiophene derivative unit **29** in solution showed two absorption maxima at 276 and 416 nm, corresponding to the S_0-S_2 and S_0-S_1 transitions, respectively. However, these bands are bathochromic shifted in the solid state. The **P(AB-3HT-borazine)** polymer showed dual absorption bands. The high-energy band at around 268 nm develops from overlapped maximum spectra of S_0-S_2 transitions of the borazine and the thiophene moieties, whereas the low-energy band (320–550 nm) is ascribed to the absorption of the thiophene derivative unit. Furthermore, no other bands have appeared at high wavelengths, suggesting that no separate charge transfer occurred at the ground state. The band gap (E_g^{opt}) of **P(AB-3HT-borazine)** polymer calculated from the absorption onsets (548 nm) in the solid state is 2.27 eV, which is close to that of AB-3HT-$(BPin)_2$ derivative (2.30 eV). Further, we have recorded emission spectra of the monomers (**9** and **21**) and the polymer (**P(AB-3HT-borazine)**) in $CHCl_3$ (λ_{exc} = 268, 276 and 416 nm, Figure 12). A well-resolved peak at 330 nm corresponding to the S_1-S_0 transition was observed when the borazine unit **9** was excited at 268 nm, whereas thiophene monomer **21** predominately gave two emission maxima at 400 and 460 nm (λ_{exc} = 276 nm), attributing to S_2-S_0 and S_1-S_0 electronic transitions, respectively. An emission maximum was obtained at 475 nm when excited at 416 nm, corresponding to S_1-S_0 electronic transition. On the other hand, broad emission spectra were obtained when the polymer was excited at 268 and 276 nm, with a maximum at 330 nm. The broad nature of the spectra obtained for the polymer is attributed to the contribution of the borazine and the thiophene moieties. The excitation of the polymer at 416 nm gave a weak emissive band between 560 and 550 nm. In addition to the broad nature of the fluorescence spectra, the emission intensities are decreased compared to those of the reference borazine and thiophene derivatives alone, suggesting the occurrence of intramolecular charge transfer (ICT).

DOI: 10.1021/acs.joc.9b01046
J. Org. Chem. 2019, 84, 9101–9116

Scheme 2. Synthetic Routes for Preparing P(AB-3HT-borazine) Polymer[a]

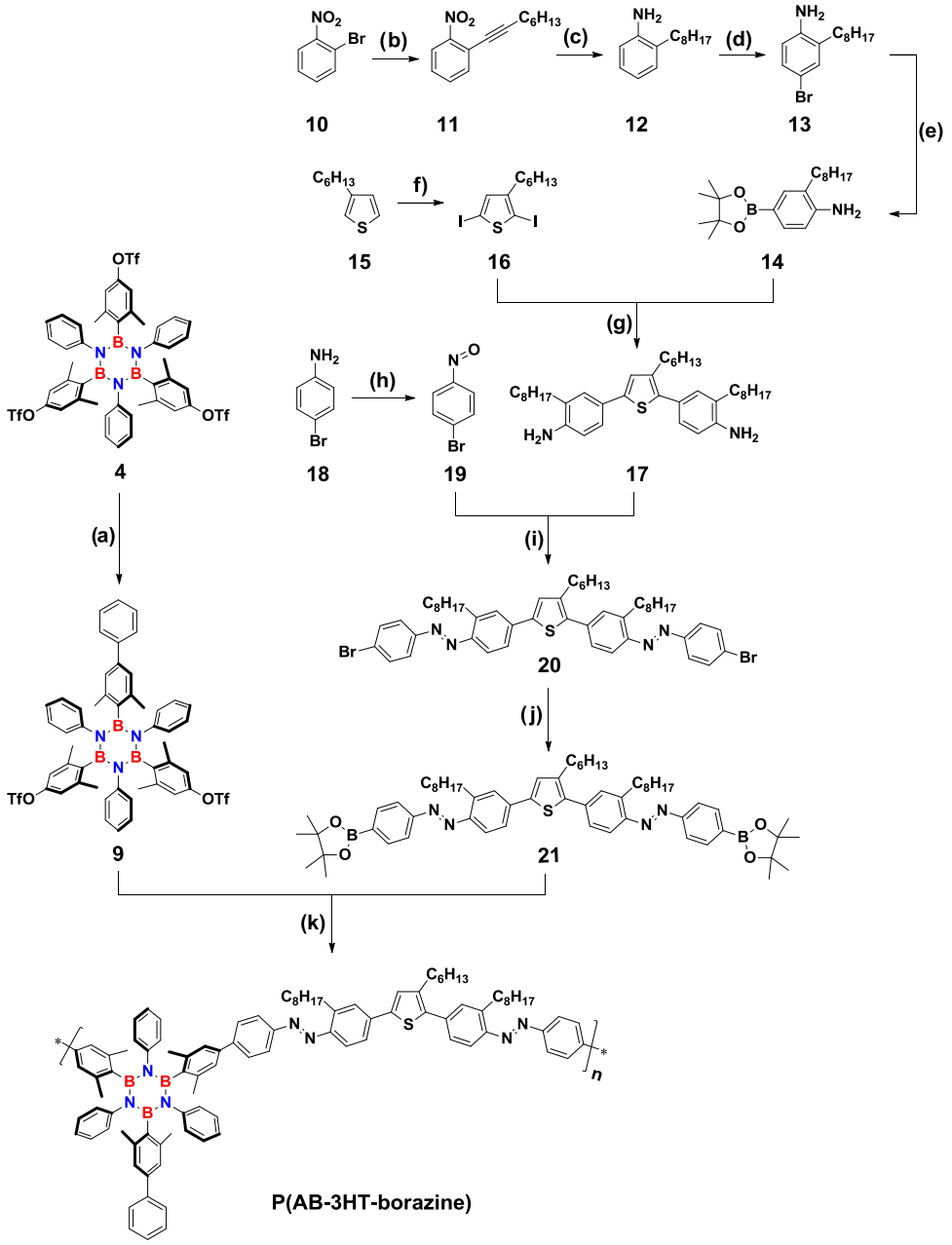

[a]Reagents and conditions: (a) Phenylboronic acid, $[Pd(PPh_3)_4]$, K_2CO_3, 1,4-dioxane/water (3:1 v/v), 100 °C, 8 h, 30%; (b) 1-octyne, $[Pd(PPh_3)_4]$, CuBr, Et_3N, 90 °C, 15 h 90%; (c) H_2 (1 atm), Pd/C (10 wt %), EtOH, rt, 6 h, 95%; (d) pyridinium hydrobromide perbromide, THF, rt, 1 h 45, 71%; (e) B_2Pin_2, $[Pd(dppf)Cl_2{\cdot}CH_2Cl_2]$, KOAc,1,4-dioxane, 90 °C, 24 h, 50%; (f) NIS, AcOH/$CHCl_3$ (3:4 v/v), rt, 24 h, 90%; (g) $[Pd(PPh_3)_4]$, K_2CO_3, 1,4-dioxane/H_2O (3:1), 105 °C, 24 h, 30%; (h) oxone, CH_2Cl_2/H_2O (1:3 v/v), rt, 3 h, quant.; (i) AcOH/EtOAc (1:1 v/v), 40 °C, 36 h, 45%; (j) B_2Pin_2, $[Pd(dppf)Cl_2{\cdot}CH_2Cl_2]$, AcOK, 1,4-dioxane, 90 °C, 24 h, 65%; (k) $[Pd(PPh_3)_4]$, K_2CO_3, toluene/water (2:0.2 v/v), 100 °C, 48 h, 60%. NIS: *N*-iodosuccinimide.

The photoswitching properties of the obtained **P(AB-3HT-borazine)** polymer were studied in $CHCl_3$ (0.025 g/L) at rt When irradiated at the maximum absorption band (440 nm), no significant changes in the absorption band were noticed (Figure 13), suggesting that the polymer does not undergo any photoinduced switching process. Considering that the band corresponding to the $\pi-\pi^*$ transition of the azo group around 360 nm is veiled by the intense S_0-S_1 transition band of the thiophene derivative unit, one can hypothesize that the lack of a selective excitation of the azobenze moieties is the main reason for the unsuccessful polymer switching. Also, it cannot be excluded that energy transfer from the excited state of the azobenzene to the oligothiophene could occur as well, quenching the photoisomerization reaction.

The good solubility of the **P(AB-3HT-borazine)** polymer in a variety of organic solvents allowed a detailed study of its solvatochromic behavior. Thus, to get an insight into the ICT nature of the **P(AB-3HT-borazine)** polymer, the solvent-dependent absorption and emission profiles (Figure 14) were recorded in cyclohexane (dielectric permittivity ε = 2.02), toluene (ε = 2.38), THF (ε = 7.58), $CHCl_3$ (ε = 4.81), MeOH (ε = 32.7), MeCN (ε = 37.5), and DMSO (ε = 46.7). A slight

DOI: 10.1021/acs.joc.9b01046
J. Org. Chem. 2019, 84, 9101−9116

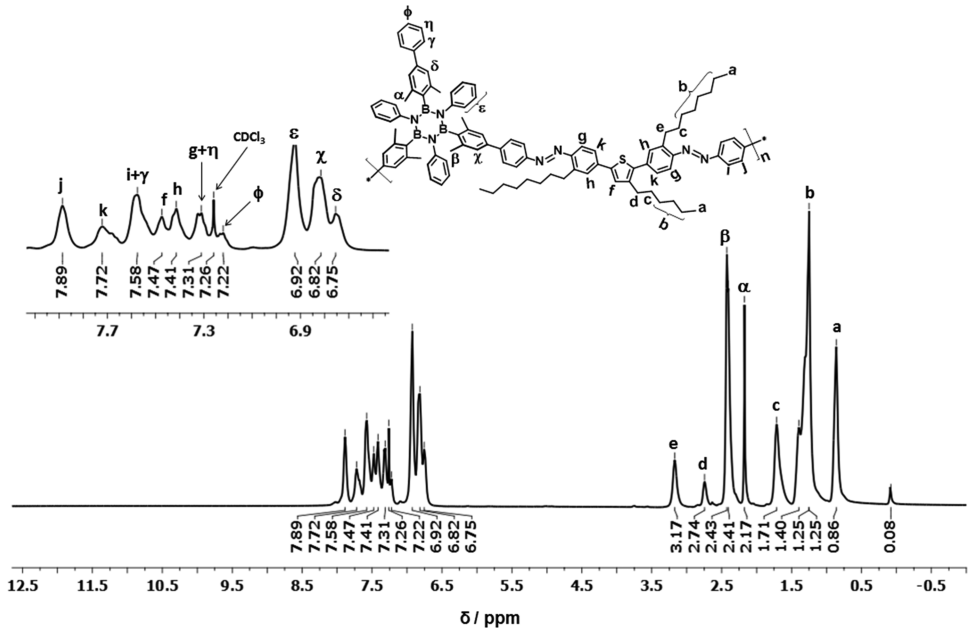

Figure 10. ^{1}H NMR spectrum of **P(AB-3HT-borazine)** polymer ($CDCl_3$, 500 MHz, 25 °C).

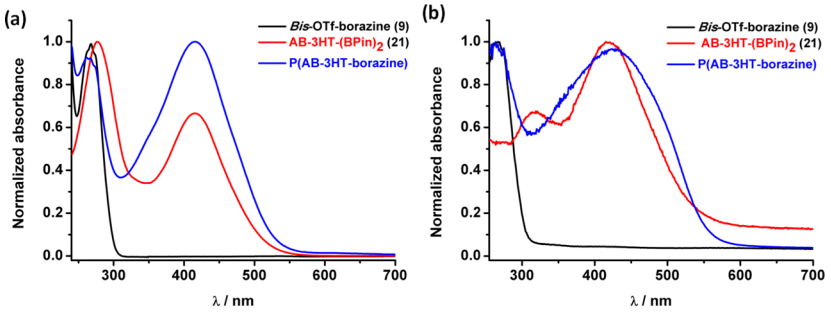

Figure 11. Normalized absorption spectra of monomers **9**, **21**, and **P(AB-3HT-borazine)** polymer in $CHCl_3$ solutions (a) and in thin films (b).

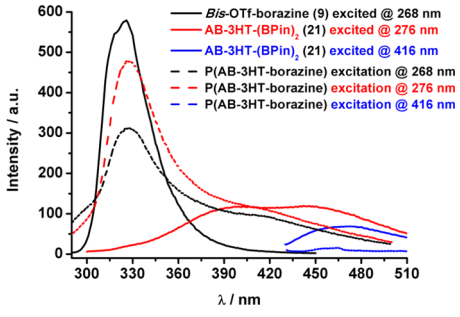

Figure 12. Emission spectra of bis-OTf-borazine **9**, AB-3HT-$(BPin)_2$ **21**, and **P(AB-3HT-borazine)** polymer recorded at rt in $CHCl_3$ (λ_{exc} = 268, 276, and 416 nm).

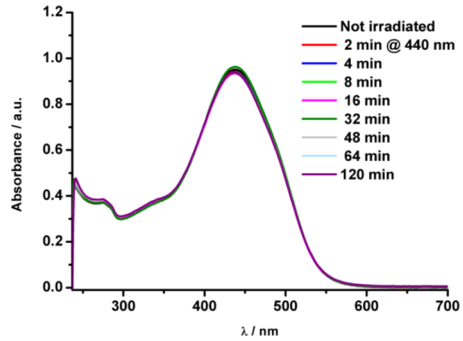

Figure 13. UV change in the absorption spectra of a 0.025 g/L solution of **P(AB-3HT-borazine)** polymer in $CHCl_3$ under irradiation at 440 nm at rt.

red-shift was observed in the absorption band maxima accompanied by a broadening of the spectra when passing from nonpolar to polar solvents (Figure 14a).[34] However, changes in the emission spectra are more pronounced (Figure 14b), with the polymer emitting at 660 and 720 nm. It is worthy to note that no significant differences were found between protic and aprotic solvents, suggesting that the hydrogen-bonding interaction is not responsible for the red-shift. The significant solvent-induced fluorescence quenching could be explained either by excited-state photoinduced intramolecular charge transfer (ICT) or by internal energy transfer or even both phenomena taking place between the borazine and thiophene units.

Cyclic voltammetry (CV) was used to investigate the electrochemical properties of the polymer **P(AB-3HT-borazine)**, along with that of its monomeric precursors bis-OTf-borazine **9** and AB-3HT-$(BPin)_2$ **21** in a solution of *n*-Bu_4NPF_6 (0.2 M) in CH_2Cl_2. As shown in Figure 15, the oxidation of borazine **9** is observed at a more anodic potential than that of the polymer and thiophene **21**. Its oxidation peak is observed at around 1.6 V, and its HOMO is determined at −5.8 eV from its

DOI: 10.1021/acs.joc.9b01046
J. Org. Chem. 2019, 84, 9101−9116

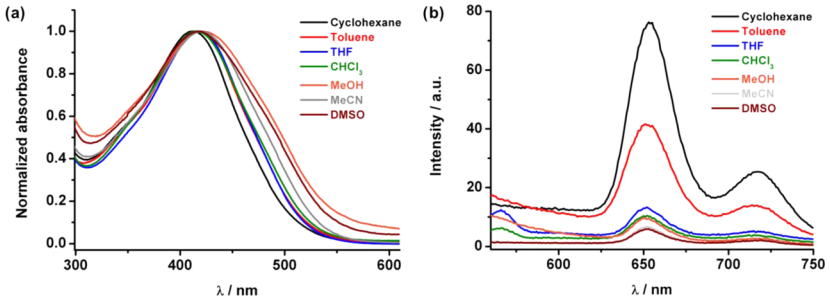

Figure 14. Absorption (a) and emission (b) spectra of the **P(AB-3HT-borazine)** polymer in various solvents of different polarities (λ_{exc} = 416 nm).

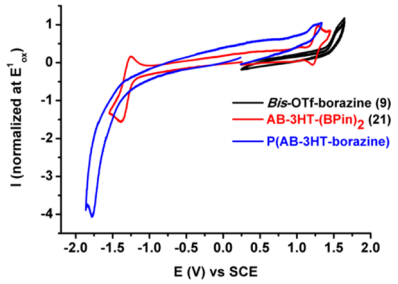

Figure 15. Cyclic voltammograms (CV) recorded in CH_2Cl_2, *n*-Bu_4NPF_6 (0.2 M), using a platinum disk working electrode (⌀ 1 mm) at a scan rate of 100 mV/s; Al_2O_3 was added to the electrolytic medium to remove water traces. CV traces of bis-OTf-borazine **9** in black, AB-3HT-$(BPin)_2$ **21** in red, and polymer **P(AB-3HT-borazine)** in blue.

onset oxidation potential E_{onset}^{ox} measured at 1.4 V. No reduction was observed before the reduction of the electrolytic medium, suggesting that this borazine has a LUMO energy level higher than −1.9 eV. The CV recorded for the AB-3HT-$(BPin)_2$ **21** presents reversible oxidation and reduction processes with E_{ox}^{1} at 1.3 V and E_{red}^{1} at −1.39 V. From $E_{onset}^{ox}/E_{onset}^{red}$, the HOMO and LUMO energy levels of AB-3HT-$(BPin)_2$ **21** were determined to be at −5.58 and −3.17 eV, respectively, resulting in an electrochemical band gap of 2.41 eV. The CV trace of the **P(AB-3HT-borazine)** polymer exhibited weak reversible oxidation (at the lowest potential value than that of the two precursors) and an irreversible reduction wave with E_{ox}^{1} and E_{red}^{1} at 1.24 and −1.78 V, respectively. The HOMO and LUMO energy levels were calculated to be −5.36 and −3.08 eV, respectively, from their onset oxidation/reduction potential values. The electrochemical band gap was calculated to be 2.28 eV, which is slightly lower than that observed for the thiophene precursors, indicating a higher conjugation length in the polymer (see also the optical band gap of 2.27 eV).

CONCLUSIONS

Owing to the possibility of functionalizing borazine cores with different groups on the aryl substituents at the N and B atoms, in this paper, we reported the use of the borazine core as a modular scaffold to prepare photoactive BNC hybrid by means of the Pd-catalyzed Suzuki cross-coupling reaction from the versatile tris-OTf-borazine derivative (**4**). Following this approach, we developed molecular BNC hybrid molecular scaffolds that, decorated with three azobenzene moieties, displayed reversible *E*/*Z* photoisomerization. The chemical structure was unveiled by X-ray diffraction analysis. The photoswitching properties of **azo-borazine-3** have been investigated by means of UV/vis spectroscopy and it exhibits efficient reversible *E*/*Z* isomerization in toluene. To further explore the chemical versatility of the borazine core, the new BN-doping polythiophene-type polymer **P(AB-3HT-borazine)** incorporating the borazine core, azobenzene, and 3HT skeletons was also developed through a Suzuki-type cross-coupling polycondensation reaction. Thermal, optical, and electrochemical properties were investigated. In particular, emission studies in solvents of different polarity suggested that the polymer undergoes intramolecular charge transfer (ICT). This work opens the gates for applying the rapidly developing borazine chemistry as a new toolbox for engineering functional materials with tailored and exploitable optoelectronic properties.

EXPERIMENTAL SECTION

General Experimental Methods. Adsorption silica chromatography columns were obtained using Merck Gerduran silica gel 60 (particle size 40−60 μm). NMR spectra (^1H, ^{13}C, ^{11}B, and ^{19}F NMR) were recorded on a 400 MHz (Jeol JNM EX-400) or 500 MHz NMR (Jeol JNM ECZR-500) spectrometer. Chemical shifts are reported in parts per million (ppm) using the solvent residual signal as an internal reference ($CDCl_3$ δ_H = 7.26 ppm, δ_C = 77.16 ppm; CD_2Cl_2 δ_H = 5.32 ppm, δ_C = 54.00 ppm; $(CD_3)_2SO$ δ_H = 2.50 ppm, δ_C = 39.52 ppm). For ^{11}B, chemical shifts are reported in ppm downfield from $BF_3{\cdot}OEt_2$ as internal reference and analyses were performed in quartz tubes. Resonance multiplicity is described as s (singlet), d (doublet), t (triplet), q (quartet), quin (quintet), m (multiplet), br (broad signal), and dd (doublet of doublets). Carbon spectra were acquired with complete decoupling for the proton. All spectra were recorded at 25 °C unless specified otherwise. Infrared spectra (IR) were recorded on a Perkin-Elmer Spectrum II FTIR System UATR, mounted with a diamond crystal. Selected absorption bands are reported in wavenumber (cm^{-1}). (i) ESI mass spectra (HRMS) were recorded on a Waters QToF2 or on a Bruker maXis Q-ToF mass spectrometer operating in positive mode at Centre de spectrométrie de masse of University of Mons and the "Fédération de Recherche" ICOA/CBM (FR2708) platform of Orléans in France. (ii) High-resolution MALDI mass spectra (HRMS) were recorded on a Waters QToF Premier mass spectrometer at Centre de spectrométrie de masse of University of Mons. Melting points (Mp) were measured on a Büchi Melting Point B-545 apparatus in an open capillary and have not been corrected. Light irradiation experiments were performed with monochromatic light produced with a LOT Oriel equipment, consisting of a 1000 W Xe lamp (LSB551 ozone free) connected via an axial optical path to a computer-controlled monochromator MSH-300. The 180° optical path was composed of a condenser lens, which collimated the light emitted from the source and a focusing lens aligned to the monochromator entrance slit. The entrance and the exit slits of the monochromator were adjusted to have a 20 nm bandwidth output light. The sample was placed in the collimated beam of the monochromatic light. UV−vis absorption spectra were recorded on a Varian Cary 5000 UV−vis−NIR spectrophotometer, using quartz cells with a path length of 1.0 cm. Emission spectra were recorded on a Cary-Varian Eclipse fluorescence spectrophotometer recorded using quartz cuvettes. All photophysical experiments were carried out in air-equilibrated solutions otherwise stated. Data collections were performed at the X-ray diffraction

DOI: 10.1021/acs.joc.9b01046
J. Org. Chem. 2019, 84, 9101−9116

beamline (XRD1) of the Elettra Synchrotron, Trieste (Italy),[35] using a Pilatus 2M hybrid-pixel area detector (DECTRIS Ltd., Baden-Daettwil, Switzerland). Complete datasets were collected at 100 K (nitrogen stream supplied through an Oxford Cryostream 700) with a monochromatic wavelength of 0.700 Å through the rotating crystal method. The crystals of compounds were dipped in N-paratone and mounted on the goniometer head with kapton loops (MiTeGen, Ithaca). Complete datasets for **4** and **3** have been obtained by merging two different data collections done on the same crystal, mounted with different orientations. The diffraction data were indexed, integrated, and scaled using XDS.[36] The structures were solved by direct methods implemented in the Sir2014 code.[37] Fourier analysis and refinement were performed by full-matrix least-squares based on F^2 implemented in SHELXL-2018/3.[38] The Coot program was used for modeling.[39] Anisotropic thermal motion was then applied to all atoms with occupancy greater than 75%. Hydrogen atoms were included at calculated positions with isotropic $U_{factors} = 1.2 \cdot U_{eq}$ or $U_{factors} = 1.5 \cdot U_{eq}$ for methyl groups (U_{eq} being the equivalent isotropic thermal factor of the bonded nonhydrogen atom). Restraints on bond lengths, angles, and thermal motions (DFIX, DANG, SIMU, and DELU) have been applied on disordered fragments. Essential crystal and refinement data are reported in the Supporting Information document (Table S1). Size exclusion chromatography (SEC or GPC) was performed in THF (with 2% triethylamine added) at 35 °C using a Polymer Laboratories liquid chromatograph equipped with a PL-DG802 degasser, an isocratic HPLC pump LC 1120 (flow rate = 1 mL/min), a Marathon autosampler (loop volume = 200 μL, solution conc. = 1 mg/mL), a PL-DRI refractive index detector, and three columns: a PL gel 10 μm guard column and two PL gel Mixed-B 10 μm columns (linear columns for separation of MWPS ranging from 500 to 106 Da). Polystyrene standards were used for calibration. Cyclic voltammetry was recorded against saturated calomel electrode in CH_2Cl_2-*n*-Bu_4NPF_6 (0.2 M) using a platinum disk working electrode (⌀ 1.0 mm) at a scan rate of 100 mV/s. Al_2O_3 was added to the electrolytic medium to avoid any water traces. Chemicals were purchased from Sigma-Aldrich, Acros Organics, Fluorochem, TCI, VWR, carbosynth, and ABCR and were used as received, unless otherwise stated. Solvents were purchased from Sigma-Aldrich, Acros Organics, and VWR, and deuterated solvents were purchased from Eurisotop. THF was distilled from Na/benzophenone and stored on activated 3 Å molecular sieves 24 h prior to use, and toluene was distilled from CaH_2 and stored on activated 3 Å molecular sieves 24 h prior to use. Aniline was purified by distillation from Sn powder, followed by distillation from Zn powder, followed by distillation from CaH_2 under an inert atmosphere, yielding a transparent colorless liquid that was stored protected from light under an argon atmosphere. Anhydrous conditions, when necessary, were achieved by keeping all glassware in the oven at 120 °C overnight and then allowed to cool down under a vacuum followed by drying the two-neck flask by flaming with a heat gun under a vacuum and purging with N_2. The inert atmosphere was maintained using N_2-filled balloons equipped with a syringe and needle that was used to penetrate the rubber stoppers used to close the flask's necks.

*4-Bromo-3,5-di-methylaniline (**5′**).* To a solution of distillated 3,5-di-methylaniline **4′** (1.2 mL, 10 mmol) in anhydrous DMF (10 mL) was added dropwise a solution of *N*-bromosuccinimide (1.8 g, 10 mmol) in anhydrous DMF (10 mL) at 0 °C. The reaction mixture was stirred at rt for 24 h. The crude was extracted with CH_2Cl_2, and the organic phases were dried over $MgSO_4$ and evaporated, yielding a brown solid, purified by column chromatography (cyclohexane/EtOAc 0−20%) to the desired product **5′** as a white solid (1.6 g, 80%). Mp: 72.7−74.1 °C. ^{1}H NMR ($CDCl_3$, 400 MHz): δ 2.32 (s, 6H), 3.54 (s, 2H), 6.44 (s, 2H). $^{13}C\{^1H\}$ NMR ($CDCl_3$, 101 MHz): δ 24.0, 115.2, 116.0, 139.0, 145.1. FTIR (UATR) ν (cm^{-1}): 3403, 3307, 2953, 2916, 1623, 1586. HRMS (EI-ToF) *m*/*z*: $[M]^+$ calcd for $C_8H_{10}BrN^+$; 198.9997; found, 198.9998.

*N,N′-Di-allyl-4-bromo-3,5-di-methylaniline (**6′**) and N,N′-Di-benzyl-4-bromo-3,5-di-methylaniline (**7′**).* 4-Bromo-3,5-dimethylaniline (1.001 g, 5 mmol), $NaHCO_3$ (1.2605 g, 15 mmol), and sodium dodecyl sulfate (20 mg) were dispersed in a mixture of EtOH and H_2O (2:5 v/v) (30 mL). R−Br (R = Allyl or R = Bn) (1 mL, 11.6 mmol) was added dropwise to the mixture. The reaction was carried out at 80 °C for 16 h. The reaction mixture was diluted with CH_2Cl_2, washed with brine and water, dried over $MgSO_4$, and evaporated to yield a brownish oil. Column chromatography (cyclohexane) purification afforded the desired product **6′** and **7′** as a transparent oil (1.34 g, 96%) and white solid (1.52 g, 80%), respectively.

*N,N′-Diallyl-4-bromo-3,5-dimethylaniline (**6′**).* ^{1}H NMR ($CDCl_3$, 400 MHz): δ 2.43 (s, 6H), 3.95 (m, 4H), 5.22−5.26 (m, 4H), 5.91 (m, 2H), 6.52 (s, 2H). $^{13}C\{^1H\}$ NMR ($CDCl_3$, 101 MHz): δ 24.4, 52.8, 112.5, 114.1, 116.1, 133.8, 138.38, 147.4. FTIR (UATR) ν (cm^{-1}): 3078, 2917, 2979, 1642, 1588, 1476, 1376, 1417, 1279, 1199, 994, 918, 823, 737. HRMS (ESI-ToF) *m*/*z*: $[M]^+$ calcd for $C_{14}H_{18}BrN^+$, 279.0623; found 279.0620.

*N,N′-Di-benzyl-4-bromo-3,5-di-methylaniline (**7′**).* Mp: 119.2−121.4 °C. ^{1}H NMR ($CDCl_3$, 400 MHz): δ 2.29 (s, 6H), 4.59 (s, 4H), 6.49 (s, 2H), 7.21 (m, 4H), 7.35 (m, 6H). $^{13}C\{^1H\}$ NMR ($CDCl_3$, 101 MHz): δ 24.4, 54.0, 112.5, 114.6, 126.8, 127.1, 128.8, 138.4, 138.7, 148.0. FTIR (UATR) ν (cm^{-1}): 3026.59, 2917.93, 1591.86, 1200.17, 1073.88, 1026.88. HRMS (ESI-ToF) *m*/*z*: $[M]^+$ calcd for $C_{22}H_{22}BrN^+$, 379.0936; found 379.0935.

*Allyl-borazine (**9′**) and Benzyl-borazine (**10′**).* The general procedure for borazine synthesis was followed:[8] Aniline (0.28 mL, 3.0 mmol) was added to anhydrous toluene (8 mL) with BCl_3 (1 M in heptane, 2.7 mL, 2.64 mmol). Ar−Li is prepared as a nucleophile from *N,N′*-di-allyl-4-bromo-3,5-di-methylaniline **6′** or *N,N′*-di-benzyl-4-bromo-3,5-di-methylaniline **7′** (0.681 g, 2.42 mmol) in anhydrous THF (10 mL) with *tert*-BuLi (1.7 M in pentane, 2.92 mL, 4.96 mmol). The yellow suspension was stirred at rt for 16 h. Solvents were removed under reduced pressure, giving a brown solid. Precipitation in cold MeOH yielded the desired compounds Allyl-borazine **9′** (0.32 g, 35%) and Benzyl-borazine **10′** (0.84 g, 70%) as white solids.

*Allyl-borazine (**9′**).* Mp: 195.5−196.9 °C, ^{1}H NMR ($CDCl_3$, 400 MHz): δ 2.14 (s, 18H), 3.65 (d, 12H), 4.92−5.02 (q, 12H), 5.65 (m, 6H), 5.93 (s, 6H), 6.67−6.75 (m, 15H). $^{13}C\{^1H\}$ NMR ($CDCl_3$, 101 MHz): δ 23.6, 52.4, 111.0, 115.9, 123.6, 126.5, 127.6, 134.7, 138.4, 146.9, 148.2. The signal for a carbon atom attached to a boron atom is missing due to quadrupolar relaxation. ^{11}B NMR ($CDCl_3$, 128 MHz): δ 36.2 (br). FTIR (UATR) ν (cm^{-1}): 3024, 2913, 1642, 1598, 1491, 1350. HRMS (MALDI-ToF) *m*/*z*: $[M]^+$ calcd for $C_{60}H_{69}B_3N_6^+$, 906.5863; found 906.5854.

*Benzyl-borazine (**10′**).* Mp: 229.8−231.8 °C. ^{1}H NMR ($CDCl_3$, 400 MHz): δ 2.15 (s, 18H), 4.35 (s, 12H), 6.03 (s, 6H), 6.87 (m, 15H), 7.02−7.04 (m, 12H), 7.19−7.28 (m, 18H). $^{13}C\{^1H\}$ NMR ($CDCl_3$, 101 MHz): δ 23.7, 53.8, 110.7, 124.1, 126.9, 127.1, 127.4, 127.7, 128.67, 139.1, 139.5. The signal for a carbon atom attached to a boron atom is missing due to quadrupolar relaxation. ^{11}B NMR ($CDCl_3$, 128 MHz): δ 36.1 (br). FTIR (UATR) ν (cm^{-1}): 3057, 1600, 1492, 1394, 1351, 1273, 1202, 1170, 1028, 964, 845, 728, 697. HRMS (ESI-ToF) *m*/*z*: $[M + H]^+$ calcd for $C_{84}H_{82}B_3N_6^+$, 1207.6875; found 1207.6841.

*Tri-amino-borazine (**11′**).* Benzyl-borazine (**10′**) (797.7 mg, 0.66 mmol) was dissolved in a mixture of CH_2Cl_2 and MeOH (85:15 v/v) (30 mL). $Pd(OH)_2$/C (20%, 161.1 mg, 1.14 mmol) was added to the solution. The suspension was hydrogenated with H_2 (1 atm) at rt for 24 h. The crude was filtrated on celite pad and evaporated to a brown residue that was purified on a neutral alumina plug (MeOH) yielding tri-amino-borazine **11′** as white powder (0.42 g, 95%). Mp: decomposition before melting around 150 °C. ^{1}H NMR ($CDCl_3$, 400 MHz): δ 2.19 (s, 18H), 6.00 (s, 6H), 6.67 (t, 3H), 6.74 (t, 6H), 6.86−6.88 (d, 6H). $^{13}C\{^1H\}$ NMR ($CDCl_3$, 101 MHz): δ 23.6, 114.8, 125.1, 127.7, 128.4, 139.6, 146.6, 148.2. The signal for a carbon atom attached to a boron atom is missing due to quadrupolar relaxation. ^{11}B NMR ($CDCl_3$, 128 MHz): δ 36.9 (br). FTIR (UATR) ν (cm^{-1}): 2913, 1599, 1491, 1491, 1452, 1355, 1307, 1164, 1074, 1026, 842, 746, 699. HRMS (ESI-ToF) *m*/*z*: $[M]^+$ calcd for $C_{42}H_{45}B_3N_6^+$, 666.3985; found 666.4021.

*(4-Bromo-3,5-dimethylphenoxy)(tert-butyl)dimethylsilane (**2**).* 4-Bromo-3,5-dimethylphenol (6.28 g, 31.20 mmol) and imidazole (6.35 g, 93.3 mmol) were dissolved in DMF (80 mL), and *tert*-butyldimethylsilyl chloride (TBDMSCl) (6.6 g, 43.68 mmol) was added. The reaction was carried out at 50 °C for 16 h. The reaction

DOI: 10.1021/acs.joc.9b01046
J. Org. Chem. 2019, 84, 9101−9116

mixture was cooled down to rt and extracted with CH_2Cl_2 (3 × 60 mL). The organic phase was dried over $MgSO_4$ and evaporated under reduced pressure at 70 °C to remove residues of TBDMSCl, yielding molecule **2** as a translucent oil (9.25 g, 94%). ^{1}H NMR ($CDCl_3$, 400 MHz): δ 0.21 (s, 6H), 1.00 (s, 9H), 2.37 (s, 6H), 6.60 (m, 2H). $^{13}C\{^1H\}$ NMR ($CDCl_3$, 100 MHz): δ −4.3, 18.3, 24.0, 25.8, 119.1, 120.0, 139.1, 154.2. FTIR (UATR) ν (cm^{-1}): 2955, 2929, 2858, 1582, 1464, 1410, 1362, 1321, 1252, 1167, 1031, 1020, 978, 834, 779, 696, 673. HRMS (ESI-ToF) m/z: $[M + H]^+$ calcd for $C_{14}H_{24}BrOSi^+$, 315.0774; found 315.0771. Characterization is in accordance with data reported in the literature.[10]

*Tri-B-(2,6-dimethyl-4-(O-TBDMS)-phenyl)-tri-N-phenyl-borazine (**3**).* Aniline (0.61 mL, 6.6 mmol) was used in anhydrous toluene (8 mL) with BCl_3 (1 M in heptane, 8 mL, 7.92 mmol). Ar−Li is prepared as a nucleophile from (4-bromo-3,5-dimethylphenoxy)(*tert*-butyl)-dimethylsilane **2** (2.46 g, 7.8 mmol) in anhydrous THF (20 mL) with *tert*-BuLi (1.7 M in pentane, 10.1 mL, 17.16 mmol). The yellow suspension was stirred at rt for 16 h. Solvents were removed under reduced pressure, affording a pale yellow solid. The mixture was poured in water (30 mL) and extracted with CH_2Cl_2 (3 × 30 mL). The organic phase was dried over $MgSO_4$ and evaporated. The crude was precipitated from cold MeOH to yield molecule **3** as white powder (1.1 g, 49%). Mp: 205−207 °C. ^{1}H NMR ($CDCl_3$, 400 MHz): δ −0.04 (s, 18H), 0.84 (s, 27H), 2.19 (s, 18H), 6.06 (m, 6H), 6.68−6.79 (m, 15H). $^{13}C\{^1H\}$ NMR ($CDCl_3$, 100 MHz): δ −4.4, 18.3, 23.1, 25.9, 117.7, 124.12 126.8, 127.2, 139.0, 146.3, 154.6. The signal for a carbon atom attached to a boron atom is missing due to quadrupolar relaxation. ^{11}B NMR ($CDCl_3$, 128 MHz): δ 36.4 (br). FTIR (UATR) ν (cm^{-1}): 3040, 2929, 1597, 1491, 1463, 1357, 1251, 1151, 1075, 1038, 1005, 968, 905, 866, 848, 836, 814, 736, 684. HRMS (ESI-ToF) m/z: $[M + H]^+$ calcd for $C_{60}H_{85}B_3N_3O_3Si_3^+$, 1012.6172; found 1012.6193. Characterization is in accordance with data reported in the literature.[10]

*Tris-OTf-borazine (**4**).* Tri-*B*-(2,6-dimethyl-4-(*O*-TBDMS)-phenyl)-tri-*N*-phenyl-borazine **3** (736.1 mg, 0.73 mmol) was dissolved in anhydrous THF (20 mL). TBAF (1 M in THF, 0.8 mL, 0.803 mmol) was added dropwise at 0 °C, a white precipitate was formed in a yellowish solution. The reaction mixture was stirred at rt for 2 h. The precipitate was then filtrated off and washed with THF (3 × 30 mL). The obtained solid was dried under vacuum and used in the following step without further purification. The obtained off-white solid from the step one (478.8 mg, 0.71 mmol) was dissolved in pyridine (30 mL), and triflic anhydride (Tf_2O) (12 equiv, 1.6 mL, 8.52 mmol) was added dropwise at 0 °C. The brownish solution was stirred at rt for 15 h. Solvents were removed under reduced pressure giving a brown solid extracted with CH_2Cl_2 (3 × 50 mL) that was purified by column chromatography (cyclohexane/CH_2Cl_2, 8:2 v/v) to afford the desired compound **4** as white powder (0.583 g, 75%). Mp: 236−238 °C. ^{1}H NMR ($CDCl_3$, 400 MHz): δ 2.32 (s, 18H), 6.49 (s, 6H), 6.75−6.77 (m, 6H), 6.80−6.82 (m, 9H). $^{13}C\{^1H\}$ NMR ($CDCl_3$, 100 MHz): δ 23.2, 27.0, 118.1, 120.3, 125.5, 126.4, 127.5, 140.4, 144.8, 149.2. The signal for a carbon atom attached to a boron atom is missing due to quadrupolar relaxation. ^{19}F NMR ($CDCl_3$, 376 MHz): δ −72.76 (s). ^{11}B NMR ($CDCl_3$, 128 MHz): δ 35.7 (br). FTIR (UATR): ν (cm^{-1}) 2924, 1590, 1492, 1419, 1364, 1240, 1207, 1121, 1013, 946, 845, 813, 769, 702. HRMS (ESI-ToF) m/z: $[M + H]^+$ calcd for $C_{45}H_{40}B_3F_9N_3O_9S_3^+$, 1066.2057; found 1066.2067. Characterization is in accordance with data reported in the literature.[10]

*(E)-1-(4-Iodophenyl)-2-phenyldiazene (**7**).* Nitrosobenzene **5** (3.0 g, 28 mmol) and 4-iodoaniline **6** (6.13 g, 28.0 mmol) were dissolved in acetic acid (50 mL). The mixture was stirred at rt for 18 h. The reaction was quenched by water (100 mL), and the orange precipitate was filtered off and washed with water. The crude was purified by column chromatography (cyclohexane), affording the desired molecule **7** as an orange solid (7.0 g, 81%). Mp: 98.2−100.4 °C. ^{1}H NMR (DMSO, 400 MHz): δ 7.59−7.62 (m, 3H), 7.67−7.69 (m, 2H), 7.89−792 (m, 2H), 7.98−8.00 (m, 2H). $^{13}C\{^1H\}$ NMR ($CDCl_3$, 100 MHz): δ 97.8, 123.1, 124.6, 129.3, 131.5; 138.5, 152.0, 152.6. FTIR (UATR) ν (cm^{-1}): 3060, 3041, 2252, 1917, 1744, 1576, 1565, 1474, 1444, 1393, 1297, 1221, 1153, 1070, 1051, 1017, 928, 907, 834, 731, 705, 689, 627. HRMS (ESI-ToF) m/z: $[M + H]^+$ calcd for $C_{12}H_{10}N_2I^+$, 308.9883; found 308.9882.

*(E)-1-Phenyl-2-(4-(4,4,5,5-tetramethyl-1,3,2-dioxaborolan-2-yl)-phenyl)diazene (**8**).* (*E*)-1-(4-Iodophenyl)-2-phenyldiazene **7** (1.6 g, 5.2 mmol), B_2Pin_2 (1.98 g, 7.8 mmol), KOAc (1.02 g, 10.4 mmol), and $[Pd(dppf)Cl_2{\cdot}CH_2Cl_2]$ (0.1272 g, 0.156 mmol) were suspended in anhydrous DMF (degassed by three freeze-to-thaw cycles) (20 mL). The reaction was carried out under an argon atmosphere at 90 °C for 18 h. After cooling down to rt, the reaction mixture was diluted with CH_2Cl_2 (60 mL), washed with brine and H_2O, dried over $MgSO_4$, and evaporated to a brown dark orange solid purified by column chromatography (cyclohexane/CH_2Cl_2, from 0 to 20%), yielding the desired compound **8** as an orange solid (1.3 g, 80%). Mp: 93.5−94.7 °C. ^{1}H NMR (CD_2Cl_2, 400 MHz): δ 1.36 (s, 12H), 7.51−7.56 (m, 3H), 7.88−7.95 (m, 6H). $^{13}C\{^1H\}$ NMR (CD_2Cl_2, 100 MHz): δ 25.1, 84.5, 122.3, 123.3, 129.5, 131.7, 135.9, 153.1, 154.7. ^{11}B NMR (CD_2Cl_2, 128 MHz): δ 29.6 (s). FTIR (UATR) ν (cm^{-1}): 3063, 2982, 2926, 1602, 1569, 1502, 1467, 1444, 1397, 1357, 1332, 1302, 1274, 1140, 1088, 1000, 963, 855. HRMS (ESI-ToF) m/z: $[M + H]^+$ calcd for $C_{18}H_{22}BN_2O_2^+$, 309.1769; found 309.1773.

Azo-borazine-3. Tris-OTf-borazine **4** (295.5 mg, 0.277 mmol), K_2CO_3 (462.0 mg, 3.328 mmol), compound **8** (341.9 mg, 1.114 mmol), and $[Pd(PPh_3)_4]$ (19.2 mg, 16.6×10^{-3} mmol) were suspended in a mixture of 1,4-dioxane and water (3:1 v/v) (16 mL) (degassed with five freeze−pump−thaw cycles) in a flame-dried 50 mL Schlenk flask. The reaction was carried out at 105 °C for 18 h. The reaction mixture was cooled down to rt, diluted with CH_2Cl_2 (100 mL), filtrated on celite, and washed with brine (100 mL) and H_2O (3 × 100 mL). The organic phase was dried over $MgSO_4$. The crude was purified by column chromatography (cyclohexane/CH_2Cl_2, from 0 to 10%), affording the desired compound **azo-borazine-3** as an orange solid (0.267 g, 83%). Mp: 270−272 °C. ^{1}H NMR (CD_2Cl_2, 400 MHz): δ 2.47 (s, 18H), 6.80−6.84 (t, 3H), 6.88−6.91 (t, 6H), 6.97 (s, 6H), 7.03−7.05 (d, 6H), 7.46−7.55 (m, 9H), 7.60−7.62 (d, 6H), 7.88−7.92 (m, 12H). $^{13}C\{^1H\}$ NMR ($CDCl_3$, 100 MHz): δ 25.0, 84.2, 93.9, 122.1, 122.9, 123.0, 123.1, 123.1, 123.6, 128.0, 129.2, 129.2, 129.3, 131.1, 131.3, 135.8. The signal for a carbon atom attached to a boron atom is missing due to quadrupolar relaxation. ^{11}B-NMR ($CDCl_3$, 128 MHz): δ 35.98 (br). FTIR (UATR) ν (cm^{-1}): 3039, 2915, 1598, 1546, 1490, 1454, 1422, 1353, 1305, 1292, 1223, 1154, 1072, 1011, 838, 792. HRMS (MALDI-ToF) m/z: $[M + H]^+$ calcd for $C_{78}H_{67}B_3N_9^+$, 1162.5793; found 1162.6010.

*Bis-OTf-borazine (**9**).* Tris-OTf-borazine **4** (200.5 mg, 0.202 mmol), K_2CO_3 (33.6 mg, 0.242 mmol), phenylboronic acid (8.2 mg, 67×10^{-3} mmol), and $[Pd(PPh_3)_4]$ (7.2 mg, 6.06×10^{-3} mmol) were suspended in a mixture of 1,4-dioxane and water (3:1, v/v) (12 mL) (degassed with five freeze−pump−thaw cycles) in a flame-dried 50 mL Schlenk flask. The reaction was carried out at 105 °C for 8 h. The reaction mixture was cooled down to rt, diluted with CH_2Cl_2 (100 mL), filtered on celite, and washed with brine (100 mL) and H_2O (3 × 100 mL). The organic phase was dried over $MgSO_4$, evaporated to a brownish solid, and purified by column chromatography (cyclohexane/CH_2Cl_2, from 0 to 10%), yielding the desired compound **9** as a white solid (0.06 g, 30%). Mp: 180.4−182.2 °C. ^{1}H NMR (CD_2Cl_2, 400 MHz,): δ 2.33 (s, 18H), 6.49 (s, 4H), 6.75−6.83 (m, 17H), 7.21 (t, 1H), 7.30 (t, 2H), 7.38−7.40 (d, 2H). $^{13}C\{^1H\}$ NMR ($CDCl_3$, 101 MHz): δ 23.3, 23.4, 118.0, 124.4, 125.1, 125.3, 126.5, 126.7, 126.8, 126.9, 127.3, 127.5, 128.6, 138.0, 139.8, 140.4, 141.2, 145.1, 145.3, 149.2. ^{19}F NMR ($CDCl_3$, 376 MHz): δ −72.75. ^{11}B NMR ($CDCl_3$, 128 MHz): δ 35.2 (br). FTIR (UATR) ν (cm^{-1}): 3040, 2923, 2854, 1590, 1492, 1454, 1419, 1363, 1310, 1240, 1208, 1142, 1120, 1075, 1013, 945, 908, 869, 845, 794, 749, 701, 582. HRMS (MALDI-ToF) m/z: $[M + H]^+$ calcd for $C_{50}H_{45}B_3N_3F_6O_6S_2^+$, 994.2969; found 994.3002.

*1-Nitro-2-(oct-1-ynyl)benzene (**11**).* 1-Bromo-2-nitrobenzene **10** (2.5 g, 12.5 mmol), 1-octyne (1.73 g, 2.4 mL, 12.5 mmol), $[Pd(PPh_3)_4]$ (288 mg, 0.25 mmol), and CuBr (73 mg, 0.5 mmol) were dissolved in freshly distilled and degassed with three freeze−pump−thaw cycles Et_3N (50 mL) in a flame-dried 100 mL Schlenk flask. The reaction was carried out at 90 °C under an argon atmosphere for 15 h. The reaction mixture was cooled down to rt, diluted with 300 mL of Et_2O, washed

DOI: 10.1021/acs.joc.9b01046
J. Org. Chem. 2019, 84, 9101−9116

with a saturated solution of NH_4Cl (3 × 100 mL) and water (3 × 100 mL), dried over $MgSO_4$, and evaporated to a dark oil. The crude product was purified by column chromatography (*n*-heptane/EtOAc, from 0 to 20%), yielding the desired compound **11** as a brownish oil (2.6 g, 90%). ^{1}H NMR ($CDCl_3$, 500 MHz): δ 0.89 (t, 3H), 1.29−1.34 (m, 4H), 1.46 (m, 2H), 1.62 (m, 2H), 2.45 (t, 2H), 7.36 (t, 1H), 7.49 (t, 1H), 7.54 (d, 1H), 7.92 (d, 1H). $^{13}C\{^1H\}$ NMR ($CDCl_3$, 126 MHz): δ 14.1,19.9, 22.6, 28.4, 28.6, 31.4, 76.0, 99.5, 119.4, 124.4, 127.9, 132.6, 134.8, 150.1. FTIR (UATR) ν (cm^{-1}): 2954, 2929, 2858, 2228, 1608, 1568, 1524, 1480, 1466, 1439, 1429, 1262, 851, 783, 744, 655. LRMS (EI-ToF) *m*/*z*: $[M]^+$ calcd for $C_{14}H_{17}NO_2^+$, 231.1259; found 231.131. Characterization is in accordance with data reported in the literature.[40]

*2-Octylaniline (**12**).* 1-Nitro-2-(oct-1-ynyl)-benzene **11** (2.24 g, 9.7 mmol) and Pd/C (10%) (222.4 mg, 0.204 mmol) were suspended in EtOH (80 mL). The reaction mixture was hydrogenated with H_2 (1 atm) at rt for 6 h. The crude was filtrated on celite and evaporated to a brown oil (1.9 g, 95%). ^{1}H NMR ($CDCl_3$, 500 MHz): δ 0.92 (t, 3H), 1.31−1.43 (m, 10H), 1.64 (m, 2H), 2.49 (t, 2H), 3.62 (s, 2H), 6.68−6.70 (d, 1H), 6.76 (t, 1H), 7.03−7.07 (m, 2H). $^{13}C\{^1H\}$ NMR ($CDCl_3$, 100 MHz): δ 14.2, 22.7, 28.8, 29.4, 29.6, 29.8, 31.4, 32.0, 115.6, 118.7, 126.8, 127.0, 129.4, 144.1. FTIR (UATR) ν (cm^{-1}): 3468, 3379, 3022, 2954, 2853, 1619, 1583, 1526, 1456, 1272, 1156. LRMS (ESI-ToF) *m*/*z*: $[M]^+$ calcd for $C_{14}H_{23}N^+$, 205.1825; found 205.1083. Characterization is in accordance with data reported in the literature.[40]

*4-Bromo-2-octylaniline (**13**).* A solution of pyridinium hydrobromide perbromide (2.33 g, 7.3 mmol) in THF (50 mL) was added dropwise over 50 min to 2-octylaniline **12** (1.50 g, 7.3 mmol) in THF (50 mL). After completion of the addition, the solution was stirred at rt for 1 h. The solution was filtered to remove the formed pyridinium hydrobromide salt. Then, the solution was treated with a saturated solution of $NaHCO_3$ (3 × 100 mL) to remove any excess of bromide, washed with water (3 × 100 mL), dried over $MgSO_4$, and evaporated to a dark oil. The crude product was purified by column chromatography (*n*-heptane/EtOAc, from 0 to 30%), yielding the desired compound **13** as a brownish oil (1.47 g, 71%). ^{1}H NMR ($CDCl_3$, 500 MHz): δ 0.91 (t, 3H), 1.30−1.42 (m, 10H), 1.60 (m, 2H), 2.43 (t, 2H), 3.61 (s, 2H), 6.53 (d, 1H), 7.11−7.12 (dd, 1H), 7.15 (d, 1H). $^{13}C\{^1H\}$ NMR ($CDCl_3$, 100 MHz): δ 13.2, 21.8, 27.5, 28.3, 28.6, 28.7, 30.2, 31.0, 109.4, 116.0, 128.2, 128.5, 130.9, 142.2. FTIR (UATR) ν (cm^{-1}): 3475, 3387, 2953, 2853, 1619, 1488, 1409, 1278, 1077. MS (GC-MS) *m*/*z*: $[M]^+$ calcd for $C_{14}H_{22}BrN^+$, 283.0936; found 283.12. Characterization is in accordance with data reported in the literature.[40]

*2-Octyl-4-(4,4,5,5-tetramethyl-1,3,2-dioxaborolan-2-yl)aniline (**14**).* 4-Bromo-2-octylaniline **13** (1.32 g, 4.62 mmol), B_2Pin_2 (1.41 g, 5.54 mmol), KOAc (1.36 g, 13.86 mmol), and $[Pd(dppf)Cl_2{\cdot}CH_2Cl_2]$ (100 mg, 0.14 mmol) were suspended in 1,4-dioxane (degassed by three freeze-to-thaw cycles) (45 mL). The reaction was carried out at 85 °C for 16 h. After cooling down to rt, the reaction mixture was diluted with EtOAc (100 mL), filtered over celite, washed with brine (2 × 100 mL) and H_2O (3 × 100 mL), dried over $MgSO_4$, and evaporated to a black oil. The crude product was purified by column chromatography (EtOAc/*n*-heptane, from 0 to 20%), yielding the molecule **14** as a brownish oil (0.765 g, 50%). ^{1}H NMR ($CDCl_3$, 500 MHz): δ 0.88 (t, 3H), 1.26−1.32 (m, 22H) (integration 34H is due to the presence of pinacolborane 12H), 1.61 (m, 2H), 2.49 (t, 2H), 3.81 (s, 2H), 6.64−6.66 (d, 1H), 7.49 (m, 2H). $^{13}C\{^1H\}$ NMR ($CDCl_3$, 101 MHz): δ 14.2, 22.8, 25.1, 29.0, 29.4, 29.6, 30.0, 31.5, 32.0, 77.0, 77.6, 77,7, 83.3, 83.6, 114.7, 125.8, 134.2, 136.5, 147.4. ^{11}B NMR ($CDCl_3$, 128 MHz): δ 29.4 (s). FTIR (UATR) ν (cm^{-1}): 3473, 3365, 2925, 1621, 1605, 1418, 1353, 1325, 1303, 1165, 1123, 1106, 1090, 964, 856. HRMS (ESI-ToF) *m*/*z*: $[M + H]^+$ calcd for $C_{20}H_{34}BNO_2^+$, 332.2755; found 332.2760. Characterization is in accordance with data reported in the literature.[40]

*3-Hexyl-2,5-diiodothiophene (**16**).* A solution of *N*-iodosuccinimide (NIS) (14.04 g, 62.4 mmol) in $CHCl_3$ (30 mL) was added dropwise to a solution of 3-hexylthiophene **15** (5.3 mL, 29.71 mmol) in a mixture of acetic acid and $CHCl_3$ (30:10 mL). The reaction mixture was stirred in dark at rt for 24 h. The reaction mixture was diluted with CH_2Cl_2 (100 mL), quenched with a saturated solution of $Na_2S_2O_3$ (50 mL), washed with H_2O (3 × 100 mL), dried over $MgSO_4$, and evaporated to a light pink oil. The crude product was purified by column chromatography (cyclohexane), affording the desired compound **16** as a colorless oil (11.2 g, 90%). ^{1}H NMR ($CDCl_3$, 400 MHz): δ 0.92 (t, 3H), 1.32 (m, 6H), 1.55 (m, 2H), 2.50 (t, 2H), 6.90 (s, 1H). $^{13}C\{^1H\}$ NMR ($CDCl_3$, 101 MHz): δ 14.3, 22.7, 28.9, 30.0, 31.7, 32.1, 76.1, 77.2, 137.8, 149.5. FTIR (UATR) ν (cm^{-1}):2953, 2923, 2853, 1525, 1464, 1395, 1190, 982, 907, 827, 724, 695, 649, 468. HRMS (ESI-ToF) *m*/*z*: $[M + H]^+$ calcd for $C_{10}H_{15}I_2S^+$, 420.8978; found 420.8961. Characterization is in accordance with data reported in the literature.[40]

*(4,4′-(3-Hexylthiophene-2,5-diyl)bis(2-octylaniline) (**17**).* 2-Octyl-4-(4,4,5,5-tetramethyl-1,3,2-dioxaborolan-2-yl)aniline **14** (520.1 mg, 1.6 mmol), 3-hexyl-2,5-diiodothiophene **16** (300.2 mg, 0.71 mmol), and K_2CO_3 (790 mg, 5.72 mmol) were dissolved in a mixture of 1,4-dioxane and H_2O (9:3 v/v) (12 mL). The reaction mixture was degassed by three freeze−pump−thaw cycles. Then, $[Pd(PPh_3)_4]$ (46.2 mg, 0.04 mmol) was added. The reaction was carried out at 105 °C for 24 h. The mixture was cooled down to rt, diluted with CH_2Cl_2 (50 mL), filtered over celite, washed with brine (2 × 100 mL) and water (2 × 100 mL), dried over $MgSO_4$, evaporated, and purified by column chromatography (cyclohexane/EtOAc, from 0 to 10%), yielding the desired compound **17** as a yellow viscous oil (0.122 g, 30%). ^{1}H NMR ($CDCl_3$, 400 MHz): δ 0.89−0.90 (t, 9H), 1.30−1.45 (m, 24H), 1.66 (m, 6H), 2.52 (t, 4H), 2.63 (t, 2H), 3.70 (s, 4H), 6.68 (q, 2H), 7.03 (s, 1H), 7.13 (s, 2H), 7.28−7.30 (m, 2H). $^{13}C\{^1H\}$ NMR ($CDCl_3$, 101 MHz): δ 14.2, 22.8, 22.8, 28.8, 28.9, 29.2, 29.4, 29.5, 29.7, 29.7, 29.8, 29.9, 31.2, 31.4, 31.5, 31.9, 32.0, 115.5, 115.9, 123.8, 124.4, 125.4, 125.8, 126.9, 127.0, 127.3, 127.8, 130.4, 136.5, 138.4, 141.9, 143.4, 143.6. FTIR (UATR) ν (cm^{-1}): 3380, 2954, 2923, 2853, 1619, 1497, 1464, 1377, 1283, 1156, 907, 816, 732, 646, 532. LRMS (ESI-ToF) *m*/*z*: $[M + H]^+$ calcd for $C_{38}H_{59}N_2S^+$, 575.4393; found 575.4331. Characterization is in accordance with data reported in the literature.[40]

*1-Bromo-4-nitrosobenzene (**19**).* A solution of oxone (7.2 g, 11.7 mmol) in water (48 mL) was added to a solution of freshly recrystallized 4-bromoaniline (1.04 g, 5.84 mmol) in CH_2Cl_2 (12 mL). The mixture was stirred at rt for 4 h. The reaction mixture was extracted with CH_2Cl_2 (3 × 20 mL) to give the desired compound **19** as a pale green solid that was used in the next step without further purification (2.15 g, quant.). ^{1}H NMR ($CDCl_3$, 400 MHz): δ 7.78 (s, 4H).

*(1E,1′E)-2,2′-((3-Hexylthiophene-2,5-diyl)bis(2-octyl-4,1-phenylene))bis(1-(4-bromophenyl)diazene) (**20**).* 1-Bromo-4-nitrosobenzene **19** (2.14 g, 11.51 mmol) and compound **17** (1.51 g, 2.63 mmol) were dissolved in a mixture of AcOH and EtOAc (1:1 v/v) (40 mL). The reaction mixture was stirred at 45 °C for 36 h. The mixture was cooled down to rt, diluted with CH_2Cl_2 (50 mL), washed with water (3 × 100 mL), dried over $MgSO_4$, evaporated, and purified by column chromatography (cyclohexane/CH_2Cl_2, from 0 to 30%), yielding the desired compound **20** as a viscous orange oil (1.08 g, 45%). ^{1}H NMR ($CDCl_3$, 500 MHz): δ 0.87 (t, 9H), 1.25−1.42 (m, 26H), 1.71 (m, 6H), 2.75 (t, 2H), 3.14−3.19 (q, 4H), 7.34 (s, 1H), 7.39−7.41 (dd, 1H), 7.48 (d, 1H), 7.52−7.54 (dd, 1H), 7.60 (d, 1H), 7.65−7.67 (m, 4H), 7.72−7.75 (d, 2H), 7.79−7.82 (m, 4H). $^{13}C\{^1H\}$ NMR ($CDCl_3$, 126 MHz): δ 14.2, 14.3, 22.8, 22.8, 29.4, 29.4, 29.6, 29.6, 29.7, 31.2, 31.6, 31.8, 31.8, 32.0, 32.3, 32.4, 115.8, 116.2, 123.8, 124.5, 124.6, 125.2, 125.3, 127.1, 127.3, 127.4, 131.1, 132.5, 132.5, 137.1, 137.7, 138.1, 141.1, 142.1, 143.8, 144.4, 149.2, 149.3, 151.9, 152.0. FTIR (UATR) ν (cm^{-1}): 2953, 2922, 2853, 1905, 1596, 1574, 1476.67, 1453, 1411, 1377, 1297, 1260, 1222, 1185, 1149, 1117, 1066, 1007, 886, 832, 722, 704. HRMS (ESI-ToF) *m*/*z*: $[M + H]^+$ calcd for $C_{50}H_{63}Br_2N_4S^+$, 909.3135; found 909.3126.

*(1E,1′E)-2,2′-((3-Hexylthiophene-2,5-diyl)bis(2-octyl-4,1-phenylene))bis(1-(4-(4,4,5,5-tetramethyl-1,3,2-dioxaborolan-2-yl)-phenyl)diazene) (AB-3HT-(BPin)$_2$) (**21**).* Compound **20** (1.00 g, 1.1 mmol), B_2Pin_2 (1.12 g, 4.41 mmol), KOAc (0.6477 g, 6.6 mmol), and $[Pd(dppf)Cl_2{\cdot}CH_2Cl_2]$ (54 mg, 0.066 mmol) were suspended in 1,4-dioxane (degassed by three freeze-to-thaw cycles) (45 mL). The reaction was carried out at 90 °C for 24 h. After cooling down to rt, the reaction mixture was diluted with CH_2Cl_2 (100 mL), filtered over celite to remove the Pd catalyst, washed with brine (2 × 100 mL) and H_2O (3 × 100 mL), dried over $MgSO_4$, and evaporated to a black oil purified by

DOI: 10.1021/acs.joc.9b01046
J. Org. Chem. 2019, 84, 9101−9116

column chromatography (cyclohexane/CH_2Cl_2, from 0 to 10%) to yield the desired compound **21** as an orange viscous oil (0.72 g, 65%). ^{1}H NMR ($CDCl_3$, 400 MHz): δ 0.87 (t, 9H), 1.27−1.38 (m, 50H), 1.73 (m, 6H), 2.75 (t, 2H), 3.18 (q, 4H), 7.34 (s, 1H), 7.40−7.42 (dd, 1H), 7.49 (d, 1H), 7.53−7.55 (dd, 1H), 7.61 (d, 1H), 7.73−7.76 (m, 2H), 7.89−7.92 (m, 4H), 7.96−7.99 (m, 4H). ^{13}C{^{1}H} NMR ($CDCl_3$, 100 MHz): δ 14.2, 14.2, 22.8, 22.8, 25.0, 25.2, 27.0, 27.1, 29.4, 29.4, 29.4, 29.6, 29.6, 29.7, 29.7, 30.3, 31.2, 31.8, 32.0, 32.3, 32.4, 43.6, 83.6, 84.2, 84.2, 115.8, 116.1, 122.2, 123.7, 127.0, 127.3, 127.3, 131.1, 135.8, 135.8, 137.0, 137.6, 138.1, 141.0, 142.1, 143.7, 144.4, 149.5, 149.6, 155.0, 155.1. Signals for the two carbon atoms attached to boron atoms are missing due to quadrupolar relaxation. ^{11}B NMR ($CDCl_3$, 128 MHz): δ 29.3 (s). FTIR (UATR) ν (cm^{-1}): 2923, 2853, 1599, 1571, 1501, 1480, 1456, 1396, 1355, 1324, 1272, 1216, 1186, 1124, 1142, 1086, 1014, 962, 886, 858, 848, 830, 736, 668, 653, 578, 540. HRMS (ESI-ToF) m/z: $[M + H]^+$ calcd for $C_{62}H_{87}B_2N_4O_4S^+$, 1005.6668; found 1005.6706.

P(AB-3HT-borazine) *Polymer.* Bis-OTf-borazine **9** (100.00 mg, 0.1 mmol), compound **21** (101.06 mg, 0.1 mmol), and K_2CO_3 (1.66 g, 1.2 mmol) were suspended in a mixture of toluene and water (2:0.2 v/v). The reaction mixture was degassed by three freeze−pump−thaw cycles. Then, $[Pd(PPh_3)_4]$ (17.33 mg, 0.015 mmol) was added. The reaction was vigorously stirred at 100 °C for 48 h. The deep-orange reaction mixture turned gradually into brown accompanied with the precipitation of a black solid. **P(AB-3HT-borazine)** polymer was obtained by purification via Soxhlet extraction for 12 h using $CHCl_3$ followed by precipitation in MeOH. The orangelike polymer was finally dried under reduced pressure at 50 °C for 24 h in 60% yield. Size exclusion chromatography (SEC) is relative to the polystyrene standard in THF (+2% Et_3N) at 30 °C: M_n = 13.2 kDa, M_w = 25.0 kDa, $Đ_M$ = 1.92, DP = 9. ^{1}H NMR ($CDCl_3$, 500 MHz): δ 0.86 (br, 9H), 1.25−1.40 (br, 50H), 1.71 (s, 6H), 2.17 (s, 6H), 2.41−2.43 (br, 12H), 2.74 (s, 2H), 3.17 (s, 4H), 6.75 (s, 1H), 6.82 (s, 4H), 6.92 (s, 15H), 7.22 (s, 1H), 7.31 (br, 4H), 7.41 (s, 2H), 7.47 (s, 1H),7.58 (br, 6H), 7.72 (br, 2H), 7.89 (s, 4H).

■ ASSOCIATED CONTENT

Supporting Information

The Supporting Information is available free of charge on the ACS Publications website at DOI: 10.1021/acs.joc.9b01046.

Synthetic schemes, copies of NMR spectra, and thermal characterization data (PDF)
Crystallographic data for compound **3** (CIF)
Crystallographic data for compound **4** (CIF)
Crystallographic data for Azo-borazine-3 (CIF)

■ AUTHOR INFORMATION

Corresponding Authors

*E-mail: olivier.coulembier@umons.ac.be (O.C.).
*E-mail: bonifazid@cardiff.ac.uk (D.B.).

ORCID

Nicola Demitri: 0000-0003-0288-3233
Joëlle Rault-Berthelot: 0000-0001-6738-8749
Olivier Coulembier: 0000-0001-5753-7851
Davide Bonifazi: 0000-0001-5717-0121

Notes

The authors declare no competing financial interest.

■ ACKNOWLEDGMENTS

The authors acknowledge the Universities of Namur and Mons for the financial support to H.O. doctoral fellowship. D.B. acknowledges the Walloon Region for the "Flycoat" and "TUBOLED" POC projects, the Science Policy Office of the Belgian Federal Government (BELSPO-IAP 7/05 project), and School of Chemistry at Cardiff University. O.C. is a Research Associate for the F.R.S. -FNRS.

■ REFERENCES

(1) (a) Nguyen, T.-T.-T.; Türp, D.; Wang, D.; Nölscher, B.; Laquai, F.; Müllen, K. A Fluorescent, Shape-Persistent Dendritic Host with Photoswitchable Guest Encapsulation and Intramolecular Energy Transfer. *J. Am. Chem. Soc.* **2011**, *133*, 11194−11204. (b) Russew, M.-M.; Hecht, S. Photoswitches: From Molecules to Materials. *Adv. Mater.* **2010**, *22*, 3348−3360. (c) Shinkai, S.; Nakaji, T.; Ogawa, T.; Shigematsu, K.; Manabe, O. Photoresponsive crown ethers. 2. Photocontrol of ion extraction and ion transport by a bis(crown ether) with a butterfly-like motion. *J. Am. Chem. Soc.* **1981**, *103*, 111−115.

(2) (a) García-Amorós, J.; Velasco, D. Recent advances towards azobenzene-based light-driven real-time information-transmitting materials. *Beilstein J. Org. Chem.* **2012**, *8*, 1003−1017. (b) Bandara, H. M. D.; Burdette, S. C. Photoisomerization in different classes of azobenzene. *Chem. Soc. Rev.* **2012**, *41*, 1809−1825. (c) Qu, D.-H.; Wang, Q.-C.; Zhang, Q.-W.; Ma, X.; Tian, H. Photoresponsive Host-Guest Functional Systems. *Chem. Rev.* **2015**, *115*, 7543−7588. (d) Hartley, G. S. The Cis-form of Azobenzene. *Nature* **1937**, *140*, 281. (e) Moreno, J.; Gerecke, M.; Grubert, L.; Kovalenko, S. A.; Hecht, S. Sensitized Two-NIR-Photon Z→E Isomerization of a Visible-Light-Addressable Bistable Azobenzene Derivative. *Angew. Chem., Int. Ed.* **2016**, *55*, 1544−1547. (f) Zeitouny, J.; Aurisicchio, C.; Bonifazi, D.; De Zorzi, R.; Geremia, S.; Bonini, M.; Palma, C.-A.; Samorì, P.; Listorti, A.; Belbakra, A.; Armaroli, N. Photoinduced structural modifications in multicomponent architectures containing azobenzene moieties as photoswitchable cores. *J. Mater. Chem.* **2009**, *19*, 4715−4724.

(3) (a) Liaros, N.; Couris, S.; Maggini, L.; De Leo, F.; Cattaruzza, F.; Aurisicchio, C.; Bonifazi, D. NLO Response of Photoswitchable Azobenzene-Based Materials. *ChemPhysChem* **2013**, *14*, 2961−2972. (b) Maggini, L.; Marangoni, T.; Georges, B.; Malicka, J. M.; Yoosaf, K.; Minoia, A.; Lazzaroni, R.; Armaroli, N.; Bonifazi, D. Azobenzene-based supramolecular polymers for processing MWCNTs. *Nanoscale* **2013**, *5*, 634−645. (c) Weber, C.; Liebig, T.; Gensler, M.; Zykov, A.; Pithan, L.; Rabe, J. P.; Hecht, S.; Bléger, D.; Kowarik, S. Cooperative Switching in Nanofibers of Azobenzene Oligomers. *Sci. Rep.* **2016**, *6*, No. 25605. (d) Bléger, D.; Ciesielski, A.; Samorì, P.; Hecht, S. Photoswitching Vertically Oriented Azobenzene Self-Assembled Monolayers at the Solid-Liquid Interface. *Chem. - Eur. J.* **2010**, *16*, 14256−14260. (e) Döbbelin, M.; Ciesielski, A.; Haar, S.; Osella, S.; Bruna, M.; Minoia, A.; Grisanti, L.; Mosciatti, T.; Richard, F.; Prasetyanto, E. A.; De Cola, L.; Palermo, V.; Mazzaro, R.; Morandi, V.; Lazzaroni, R.; Ferrari, A. C.; Beljonne, D.; Samorì, P. Light-enhanced liquid-phase exfoliation and current photoswitching in graphene-azobenzene composites. *Nat. Commun.* **2016**, *7*, No. 11090. (f) Castellanos, S.; Goulet-Hanssens, A.; Zhao, F.; Dikhtiarenko, A.; Pustovarenko, A.; Hecht, S.; Gascon, J.; Kapteijn, F.; Bléger, D. Structural Effects in Visible-Light-Responsive Metal-Organic Frameworks Incorporating ortho-Fluoroazobenzenes. *Chem. - Eur. J.* **2016**, *22*, 746−752. (g) Mahesh, S.; Gopal, A.; Thirumalai, R.; Ajayaghosh, A. Light-Induced Ostwald Ripening of Organic Nanodots to Rods. *J. Am. Chem. Soc.* **2012**, *134*, 7227−7230.

(4) (a) Velema, W. A.; Szymanski, W.; Feringa, B. L. Photopharmacology: Beyond Proof of Principle. *J. Am. Chem. Soc.* **2014**, *136*, 2178−2191. (b) Broichhagen, J.; Frank, J. A.; Trauner, D. A Roadmap to Success in Photopharmacology. *Acc. Chem. Res.* **2015**, *48*, 1947−1960. (c) Woolley, G. A. Photocontrolling Peptide α Helices. *Acc. Chem. Res.* **2005**, *38*, 486−493. (d) Schütt, M.; Krupka, S. S.; Milbradt, A. G.; Deindl, S.; Sinner, E.-K.; Oesterhelt, D.; Renner, C.; Moroder, L. Photocontrol of Cell Adhesion Processes: Model Studies with Cyclic Azobenzene-RGD Peptides. *Chem. Biol.* **2003**, *10*, 487−490. (e) Stein, M.; Middendorp, S. J.; Carta, V.; Pejo, E.; Raines, D. E.; Forman, S. A.; Sigel, E.; Trauner, D. Azo-Propofols: Photochromic Potentiators of GABAA Receptors. *Angew. Chem., Int. Ed.* **2012**, *51*, 10500−10504. (f) Aemissegger, A.; Kräutler, V.; van Gunsteren, W. F.; Hilvert, D. A Photoinducible β-Hairpin. *J. Am. Chem. Soc.* **2005**, *127*, 2929−2936.

(5) (a) Engel, S.; Möller, N.; Ravoo, B. J. Stimulus-Responsive Assembly of Nanoparticles using Host-Guest Interactions of Cyclodextrins. *Chem. - Eur. J.* **2018**, *24*, 4741−4748. (b) Tomatsu, I.; Hashidzume, A.; Harada, A. Photoresponsive Hydrogel System Using

DOI: 10.1021/acs.joc.9b01046
J. Org. Chem. 2019, 84, 9101−9116

Molecular Recognition of α-Cyclodextrin. *Macromolecules* **2005**, *38*, 5223−5227. (c) Yamaguchi, H.; Kobayashi, Y.; Kobayashi, R.; Takashima, Y.; Hashidzume, A.; Harada, A. Photoswitchable gel assembly based on molecular recognition. *Nat. Commun.* **2012**, *3*, No. 603. (d) Goswami, S.; Ghosh, K.; Halder, M. Molecular recognition: Hydrogen bonding induced configurational locking of a new photoresponsive receptor by dicarboxylic acids. *Tetrahedron Lett.* **1999**, *40*, 1735−1738. (e) Goodman, A.; Breinlinger, E.; Ober, M.; Rotello, V. M. Controlled Multi-Stage Recognition of Guests Using Orthogonal Electro- and Photochemical Inputs. *J. Am. Chem. Soc.* **2001**, *123*, 6213−6214. (f) Dąbrowa, K.; Niedbała, P.; Jurczak, J. Anion-tunable control of thermal Z-E isomerisation in basic azobenzene receptors. *Chem. Commun.* **2014**, *50*, 15748−15751. (g) Lohse, M.; Nowosinski, K.; Traulsen, N. L.; Achazi, A. J.; von Krbek, L. K. S.; Paulus, B.; Schalley, C. A.; Hecht, S. Gating the photochromism of an azobenzene by strong host-guest interactions in a divalent pseudo[2]-rotaxane. *Chem. Commun.* **2015**, *51*, 9777−9780. (h) Arroyave, F. A.; Ballester, P. Reversible Light-Controlled Cargo Release in Hydrogen-Bonded Dimeric Capsules. *J. Org. Chem.* **2015**, *80*, 10866−10873. (i) Cafeo, G.; Kohnke, F. H.; Mezzatesta, G.; Profumo, A.; Rosano, C.; Villari, A.; White, A. J. P. Host-Guest Chemistry of a Bis-Calix[4]-pyrrole Derivative Containing a trans/cis-Switchable Azobenzene Unit with Several Aliphatic Bis-Carboxylates. *Chem. - Eur. J.* **2015**, *21*, 5323−5327. (j) Vulcano, R.; Pengo, P.; Velari, S.; Wouters, J.; De Vita, A.; Tecilla, P.; Bonifazi, D. Toward Fractioning of Isomers through Binding-Induced Acceleration of Azobenzene Switching. *J. Am. Chem. Soc.* **2017**, *139*, 18271−18280.

(6) (a) Huang, J.; Li, Y. BN Embedded Polycyclic π-Conjugated Systems: Synthesis, Optoelectronic Properties, and Photovoltaic Applications. *Front. Chem.* **2018**, *6*, No. 341. (b) Bosdet, M. J. D.; Piers, W. E. B-N as a C-C substitute in aromatic systems. *Can. J. Chem.* **2009**, *87*, 8−29. (c) Campbell, P. G.; Marwitz, A. J. V.; Liu, S.-Y. Recent Advances in Azaborine Chemistry. *Angew. Chem., Int. Ed.* **2012**, *51*, 6074−6092. (d) Helten, H. B═N Units as Part of Extended π-Conjugated Oligomers and Polymers. *Chem. - Eur. J.* **2016**, *22*, 12972−12982. (e) Lorenzo-García, M. M.; Bonifazi, D. Renaissance of an Old Topic: From Borazines to BN-doped Nanographenes. *CHIMIA Int. J. Chem.* **2017**, *71*, 550−557. (f) Hatakeyama, T.; Hashimoto, S.; Seki, S.; Nakamura, M. Synthesis of BN-Fused Polycyclic Aromatics via Tandem Intramolecular Electrophilic Arene Borylation. *J. Am. Chem. Soc.* **2011**, *133*, 18614−18617. (g) Morgan, M. M.; Piers, W. E. Efficient synthetic methods for the installation of boron-nitrogen bonds in conjugated organic molecules. *Dalton Trans.* **2016**, *45*, 5920−5924.

(7) (a) Stock, A.; Pohland, E. Borwasserstoffe, VIII. Zur Kenntnis des B_2H_6 und des B_5H_{11}. *Ber. Dtsch. Chem. Ges.* **1926**, *59*, 2210−2215. (b) Wiberg, E.; Bolz, A. Das "anorganische Benzol" $B_3N_3H_6$. *Ber. Dtsch. Chem. Ges.* **1940**, *73*, 209−232. (c) Kiran, B.; Phukan, A. K.; Jemmis, E. D. Is Borazine Aromatic? Unusual Parallel Behavior between Hydrocarbons and Corresponding B-N Analogues. *Inorg. Chem.* **2001**, *40*, 3615−3618. (d) Bonifazi, D.; Fasano, F.; Lorenzo-Garcia, M. M.; Marinelli, D.; Oubaha, H.; Tasseroul, J. Boron-nitrogen doped carbon scaffolding: organic chemistry, self-assembly and materials applications of borazine and its derivatives. *Chem. Commun.* **2015**, *51*, 15222−15236.

(8) Kervyn, S.; Fenwick, O.; Di Stasio, F.; Shin, Y. S.; Wouters, J.; Accorsi, G.; Osella, S.; Beljonne, D.; Cacialli, F.; Bonifazi, D. Polymorphism, Fluorescence, and Optoelectronic Properties of a Borazine Derivative. *Chem. - Eur. J.* **2013**, *19*, 7771−7779.

(9) (a) Schwarz, M.; Garnica, M.; Fasano, F.; Demitri, N.; Bonifazi, D.; Auwärter, W. BN-Patterning of Metallic Substrates through Metal Coordination of Decoupled Borazines. *Chem. - Eur. J.* **2018**, *24*, 9565−9571. (b) Auwärter, W. Hexagonal boron nitride monolayers on metal supports: Versatile templates for atoms, molecules and nanostructures. *Surf. Sci. Rep.* **2018**, 1−95.

(10) (a) Marinelli, D.; Fasano, F.; Najjari, B.; Demitri, N.; Bonifazi, D. Borazino-Doped Polyphenylenes. *J. Am. Chem. Soc.* **2017**, *139*, 5503−5519. (b) Dosso, J.; Marinelli, D.; Demitri, N.; Bonifazi, D. Structural Properties of Highly Doped Borazino Polyphenylenes Obtained through Condensation Reaction. *ACS Omega* **2019**, *4*, 9343−9351.

(11) Dosso, J.; Tasseroul, J.; Fasano, F.; Marinelli, D.; Biot, N.; Fermi, A.; Bonifazi, D. Synthesis and Optoelectronic Properties of Hexa-perihexabenzoborazinocoronene. *Angew. Chem., Int. Ed.* **2017**, *56*, 4483−4487.

(12) (a) Riensch, N. A.; Deniz, A.; Kühl, S.; Müller, L.; Adams, A.; Pich, A.; Helten, H. Borazine-based inorganic-organic hybrid cyclomatrix microspheres by silicon/boron exchange precipitation polycondensation. *Polym. Chem.* **2017**, *8*, 5264−5268. (b) Reich, T. E.; Jackson, K. T.; Li, S.; Jena, P.; El-Kaderi, H. M. Synthesis and characterization of highly porous borazine-linked polymers and their performance in hydrogen storage application. *J. Mater. Chem.* **2011**, *21*, 10629−10632. (c) Reich, T. E.; Behera, S.; Jackson, K. T.; Jena, P.; El-Kaderi, H. M. Highly selective CO_2/CH_4 gas uptake by a halogen-decorated borazine-linked polymer. *J. Mater. Chem.* **2012**, *22*, 13524−13528.

(13) (a) Wang, X.-Y.; Zhuang, F.-D.; Wang, R.-B.; Wang, X.-C.; Cao, X.-Y.; Wang, J.-Y.; Pei, J. A Straightforward Strategy toward Large BN-Embedded π-Systems: Synthesis, Structure, and Optoelectronic Properties of Extended BN Heterosuperbenzenes. *J. Am. Chem. Soc.* **2014**, *136*, 3764−3767. (b) Yang, D.-T.; Shi, Y.; Peng, T.; Wang, S. BN-Heterocycles Bearing Two BN Units: Influence of the Linker and the Location of BN Units on Electronic Properties and Photoreactivity. *Organometallics* **2017**, *36*, 2654−2660. (c) Sawahata, H.; Maruyama, M.; Cuong Nguyen, T.; Omachi, H.; Shinohara, H.; Okada, S. Band-Gap Engineering of Graphene Heterostructures by Substitutional Doping with B_3N_3. *ChemPhysChem* **2018**, *19*, 237−242. (d) Baggett, A. W.; Guo, F.; Li, B.; Liu, S.-Y.; Jäkle, F. Regioregular Synthesis of Azaborine Oligomers and a Polymer with a *syn* Conformation Stabilized by N-H···π Interactions. *Angew. Chem., Int. Ed.* **2015**, *54*, 11191−11195. (e) van de Wouw, H. L.; Lee, J. Y.; Awuyah, E. C.; Klausen, R. S. A BN Aromatic Ring Strategy for Tunable Hydroxy Content in Polystyrene. *Angew. Chem., Int. Ed.* **2018**, *57*, 1673−1677. (f) Wan, W.-M.; Baggett, A. W.; Cheng, F.; Lin, H.; Liu, S.-Y.; Jäkle, F. Synthesis by free radical polymerization and properties of BN-polystyrene and BN-poly(vinylbiphenyl). *Chem. Commun.* **2016**, *52*, 13616−13619.

(14) (a) Dou, C.; Ding, Z.; Zhang, Z.; Xie, Z.; Liu, J.; Wang, L. Developing Conjugated Polymers with High Electron Affinity by Replacing a C-C Unit with a B←N Unit. *Angew. Chem., Int. Ed.* **2015**, *54*, 3648−3652. (b) Lorenz, T.; Lik, A.; Plamper, F. A.; Helten, H. Dehydrocoupling and Silazane Cleavage Routes to Organic-Inorganic Hybrid Polymers with NBN Units in the Main Chain. *Angew. Chem., Int. Ed.* **2016**, *55*, 7236−7241. (c) Lorenz, T.; Crumbach, M.; Eckert, T.; Lik, A.; Helten, H. Poly(p-phenylene iminoborane): A Boron-Nitrogen Analogue of Poly(p-phenylene vinylene). *Angew. Chem., Int. Ed.* **2017**, *56*, 2780−2784. (d) Wang, X.-Y.; Zhuang, F.-D.; Wang, J.-Y.; Pei, J. Incorporation of polycyclic azaborine compounds into polythiophene-type conjugated polymers for organic field-effect transistors. *Chem. Commun.* **2015**, *51*, 17532−17535. (e) Ayhan, O.; Eckert, T.; Plamper, F. A.; Helten, H. Poly(iminoborane)s: An Elusive Class of Main-Group Polymers? *Angew. Chem., Int. Ed.* **2016**, *55*, 13321−13325. (f) Ayhan, O.; Riensch, N. A.; Glasmacher, C.; Helten, H. Cyclolinear Oligo- and Poly(iminoborane)s: The Missing Link in Inorganic Main-Group Macromolecular Chemistry. *Chem. - Eur. J.* **2018**, *24*, 5883−5894.

(15) (a) Moliton, A.; Hiorns, R. C. Review of electronic and optical properties of semiconducting π-conjugated polymers: applications in optoelectronics. *Polym. Int.* **2004**, *53*, 1397−1412. (b) Heeger, A. J. Semiconducting polymers: the Third Generation. *Chem. Soc. Rev.* **2010**, *39*, 2354−2371. (c) Facchetti, A. π-Conjugated Polymers for Organic Electronics and Photovoltaic Cell Applications. *Chem. Mater.* **2011**, *23*, 733−758. (d) Dou, L.; You, J.; Hong, Z.; Xu, Z.; Li, G.; Street, R. A.; Yang, Y. 25th Anniversary Article: A Decade of Organic/Polymeric Photovoltaic Research. *Adv. Mater.* **2013**, *25*, 6642−6671. (e) Shirakawa, H.; Louis, E. J.; MacDiarmid, A. G.; Chiang, C. K.; Heeger, A. J. Synthesis of electrically conducting organic polymers: halogen derivatives of polyacetylene, (CH). *J. Chem. Soc., Chem. Commun.* **1977**, 578−580.

DOI: 10.1021/acs.joc.9b01046
J. Org. Chem. 2019, 84, 9101−9116

(16) (a) Facchetti, A. Π-conjugated polymers for organic electronics and photovoltaic cell applications. *Chem. Mater.* **2011**, *23*, 733−758. (b) Zhang, Z.; Liao, M.; Lou, H.; Hu, Y.; Sun, X.; Peng, H. Conjugated Polymers for Flexible Energy Harvesting and Storage. *Adv. Mater.* **2018**, *30*, No. 1704261. (c) Swager, T. M. 50th Anniversary Perspective: Conducting/Semiconducting Conjugated Polymers. A Personal Perspective on the Past and the Future. *Macromolecules* **2017**, *50*, 4867−4886. (d) Wang, C.; Dong, H.; Hu, W.; Liu, Y.; Zhu, D. Semiconducting π-conjugated systems in field-effect transistors: a material odyssey of organic electronics. *Chem. Rev.* **2012**, *112*, 2208−2267.

(17) (a) Takimiya, K.; Osaka, I.; Nakano, M. π-Building Blocks for Organic Electronics: Revaluation of "Inductive" and "Resonance" Effects of π-Electron Deficient Units. *Chem. Mater.* **2014**, *26*, 587−593. (b) Li, G.; Chang, W.-H.; Yang, Y. Low-bandgap conjugated polymers enabling solution-processable tandem solar cells. *Nat. Rev. Mater.* **2017**, *2*, No. 17043.

(18) (a) Edel, K.; Brough, S. A.; Lamm, A. N.; Liu, S.-Y.; Bettinger, H. F. 1,2-Azaborine: The Boron-Nitrogen Derivative of ortho-Benzyne. *Angew. Chem., Int. Ed.* **2015**, *54*, 7819−7822. (b) Noda, H.; Furutachi, M.; Asada, Y.; Shibasaki, M.; Kumagai, N. Unique physicochemical and catalytic properties dictated by the B_3NO_2 ring system. *Nat. Chem.* **2017**, *9*, 571.

(19) (a) Jäkle, F. Advances in the Synthesis of Organoborane Polymers for Optical, Electronic, and Sensory Applications. *Chem. Rev.* **2010**, *110*, 3985−4022. (b) Snyder, J. A.; Grüninger, P.; Bettinger, H. F.; Bragg, A. E. Excited-State Deactivation Pathways and the Photocyclization of BN-Doped Polyaromatics. *J. Phys. Chem. A* **2017**, *121*, 5136−5146. (c) Dou, C.; Long, X.; Ding, Z.; Xie, Z.; Liu, J.; Wang, L. An Electron-Deficient Building Block Based on the B←N Unit: An Electron Acceptor for All-Polymer Solar Cells. *Angew. Chem., Int. Ed.* **2016**, *55*, 1436−1440.

(20) (a) Chen, D.-M.; Qin, Q.; Sun, Z.-B.; Peng, Q.; Zhao, C.-H. Synthesis and properties of B,N-bridged p-terphenyls. *Chem. Commun.* **2014**, *50*, 782−784. (b) Müller, M.; Behnle, S.; Maichle-Mössmer, C.; Bettinger, H. F. Boron-nitrogen substituted perylene obtained through photocyclisation. *Chem. Commun.* **2014**, *50*, 7821−7823.

(21) Wakamiya, A.; Ide, T.; Yamaguchi, S. Toward π-Conjugated Molecule Bundles: Synthesis of a Series of B,B′,B″-Trianthryl-N,N′,N″-triarylborazines and the Bundle Effects on Their Properties. *J. Am. Chem. Soc.* **2005**, *127*, 14859−14866.

(22) (a) Holliday, S.; Donaghey, J. E.; McCulloch, I. Advances in Charge Carrier Mobilities of Semiconducting Polymers Used in Organic Transistors. *Chem. Mater.* **2014**, *26*, 647−663. (b) Arias, A. C.; MacKenzie, J. D.; McCulloch, I.; Rivnay, J.; Salleo, A. Materials and Applications for Large Area Electronics: Solution-Based Approaches. *Chem. Rev.* **2010**, *110*, 3−24. (c) Bhatt, M. P.; Magurudeniya, H. D.; Rainbolt, E. A.; Huang, P.; Dissanayake, D. S.; Biewer, M. C.; Stefan, M. C. Poly(3-Hexylthiophene) Nanostructured Materials for Organic Electronics Applications. *J. Nanosci. Nanotechnol.* **2014**, *14*, 1033−1050.

(23) (a) Kalashnyk, N.; Ganesh Nagaswaran, P.; Kervyn, S.; Riello, M.; Moreton, B.; Jones, T. S.; De Vita, A.; Bonifazi, D.; Costantini, G. Self-Assembly of Decoupled Borazines on Metal Surfaces: The Role of the Peripheral Groups. *Chem. - Eur. J.* **2014**, *20*, 11856−11862. (b) Kervyn, S.; Kalashnyk, N.; Riello, M.; Moreton, B.; Tasseroul, J.; Wouters, J.; Jones, T. S.; De Vita, A.; Costantini, G.; Bonifazi, D. "Magic" Surface Clustering of Borazines Driven by Repulsive Intermolecular Forces. *Angew. Chem., Int. Ed.* **2013**, *52*, 7410−7414.

(24) Groszos, S. J.; Stafiej, S. F. Organoboron Compounds. I. A New Synthesis of B-Trialkyl and Triaryl-N-triphenylborazoles1. *J. Am. Chem. Soc.* **1958**, *80*, 1357−1360.

(25) Smith, B. C.; Thakur, L. Boron-Nitrogen Bond Strengths in Borazoles. *Nature* **1965**, *208*, 74−75.

(26) (a) Vogtle, F.; Gorka, M.; Hesse, R.; Ceroni, P.; Maestri, M.; Balzani, V. Photochemical and photophysical properties of poly-(propylene amine) dendrimers with peripheral naphthalene and azobenzene groups. *Photochem. Photobiol. Sci.* **2002**, *1*, 45−51. (b) Conti, I.; Garavelli, M.; Orlandi, G. The Different Photoisomerization Efficiency of Azobenzene in the Lowest nπ* and ππ* Singlets: The Role of a Phantom State. *J. Am. Chem. Soc.* **2008**, *130*, 5216−5230.

(27) Wei-Guang Diau, E. A New Trans-to-Cis Photoisomerization Mechanism of Azobenzene on the S1(n,π*) Surface. *J. Phys. Chem. A* **2004**, *108*, 950−956.

(28) Yoon, S.-J.; Chung, J. W.; Gierschner, J.; Kim, K. S.; Choi, M.-G.; Kim, D.; Park, S. Y. Multistimuli Two-Color Luminescence Switching via Different Slip-Stacking of Highly Fluorescent Molecular Sheets. *J. Am. Chem. Soc.* **2010**, *132*, 13675−13683.

(29) (a) Spano, F. C.; Silva, C. H- and J-Aggregate Behavior in Polymeric Semiconductors. *Annu. Rev. Phys. Chem.* **2014**, *65*, 477−500. (b) Carminati, R.; Greffet, J. J.; Henkel, C.; Vigoureux, J. M. Radiative and non-radiative decay of a single molecule close to a metallic nanoparticle. *Opt. Commun.* **2006**, *261*, 368−375. (c) Chen, J.; Law, C. C. W.; Lam, J. W. Y.; Dong, Y.; Lo, S. M. F.; Williams, I. D.; Zhu, D.; Tang, B. Z. Synthesis, Light Emission, Nanoaggregation, and Restricted Intramolecular Rotation of 1,1-Substituted 2,3,4,5-Tetraphenylsiloles. *Chem. Mater.* **2003**, *15*, 1535−1546. (d) Hong, Y.; Lam, J. W. Y.; Tang, B. Z. Aggregation-induced emission. *Chem. Soc. Rev.* **2011**, *40*, 5361−5388.

(30) (a) Hong, Y.; Lam, J. W. Y.; Tang, B. Z. Aggregation-induced emission: phenomenon, mechanism and applications. *Chem. Commun.* **2009**, 4332−4353. (b) Xu, B.; He, J.; Dong, Y.; Chen, F.; Yu, W.; Tian, W. Aggregation emission properties and self-assembly of conjugated oligocarbazoles. *Chem. Commun.* **2011**, *47*, 6602−6604.

(31) Han, M.; Cho, S. J.; Norikane, Y.; Shimizu, M.; Kimura, A.; Tamagawa, T.; Seki, T. Multistimuli-responsive azobenzene nanofibers with aggregation-induced emission enhancement characteristics. *Chem. Commun.* **2014**, *50*, 15815−15818.

(32) (a) Horn, D.; Rieger, J. Organic Nanoparticles in the Aqueous Phase-Theory, Experiment, and Use. *Angew. Chem., Int. Ed.* **2001**, *40*, 4330−4361. (b) Yin, Y.; Alivisatos, A. P. Colloidal nanocrystal synthesis and the organic-inorganic interface. *Nature* **2005**, *437*, 664−670.

(33) Davey, M.; Lee, V.; Miller, R.; Marks, T. J. Synthesis of aryl nitroso derivatives by tert-butyl hypochlorite oxidation in homogeneous media. Intermediates for the preparation of high-hyperpolarizability chromophore skeletons. *J. Org. Chem.* **1999**, *64*, 4976−4979.

(34) (a) Dias, F. B.; Pollock, S.; Hedley, G.; Pålsson, L.-O.; Monkman, A.; Perepichka, I. I.; Perepichka, I. F.; Tavasli, M.; Bryce, M. R. Intramolecular Charge Transfer Assisted by Conformational Changes in the Excited State of Fluorene-dibenzothiophene-S,S-dioxide Co-oligomers. *J. Phys. Chem. B* **2006**, *110*, 19329−19339. (b) Pop, F.; Riobé, F.; Seifert, S.; Cauchy, T.; Ding, J.; Dupont, N.; Hauser, A.; Koch, M.; Avarvari, N. Tetrathiafulvalene-1,3,5-triazines as (Multi)-Donor-Acceptor Systems with Tunable Charge Transfer: Structural, Photophysical, and Theoretical Investigations. *Inorg. Chem.* **2013**, *52*, 5023−5034.

(35) Lausi, A.; Polentarutti, M.; Onesti, S.; Plaisier, J. R.; Busetto, E.; Bais, G.; Barba, L.; Cassetta, A.; Campi, G.; Lamba, D.; Pifferi, A.; Mande, S. C.; Sarma, D. D.; Sharma, S. M.; Paolucci, G. Status of the crystallography beamlines at Elettra. *Eur. Phys. J. Plus* **2015**, *130*, 43.

(36) Kabsch, W. XDS. *Acta Crystallogr., Sect. D: Biol. Crystallogr.* **2010**, *66*, 125−132.

(37) Burla, M. C.; Caliandro, R.; Carrozzini, B.; Cascarano, G. L.; Cuocci, C.; Giacovazzo, C.; Mallamo, M.; Mazzone, A.; Polidori, G. Crystal structure determination and refinement via SIR2014. *J. Appl. Crystallogr.* **2015**, *48*, 306−309.

(38) Sheldrick, G. Crystal structure refinement with SHELXL. *Acta Crystallogr., Sect. C: Struct. Chem.* **2015**, *71*, 3−8.

(39) Emsley, P.; Lohkamp, B.; Scott, W. G.; Cowtan, K. Features and development of Coot. *Acta Crystallogr., Sect. D: Biol. Crystallogr.* **2010**, *66*, 486−501.

(40) Nguyen, H. T.; Coulembier, O.; Gheysen, K.; Martins, J. C.; Dubois, P. Copper-Catalyzed Dehydrogenative Polycondensation of a Bis-Aniline Hexylthiophene-Based Monomer: A Kinetically Controlled Air-Tolerant Process. *Macromolecules* **2012**, *45*, 9547−9550.

DOI: 10.1021/acs.joc.9b01046
J. Org. Chem. 2019, 84, 9101−9116